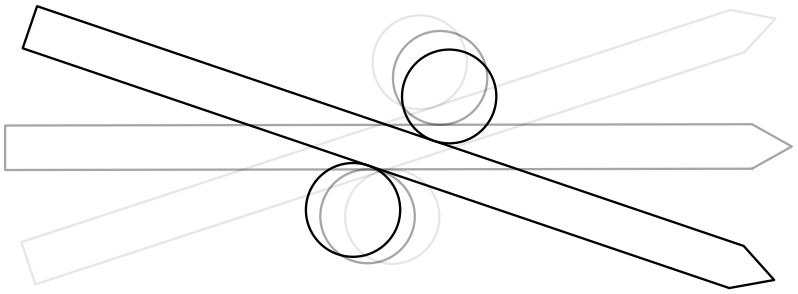

Dexterity in Robotic Grasping

Object Oscillation

José Maria Rosa Alves

Thesis to obtain the Master of Science Degree in

Mechanical Engineering

Supervisor: Prof. Jorge Manuel Mateus Martins

Examination Committee

Chairperson: Prof. Carlos Baptista Cardeira

Supervisor: Prof. Jorge Manuel Mateus Martins

Member of the Committee: Prof. Miguel Afonso Dias de Ayala Botto

December 2021

Acknowledgments

I would like to express my gratitude to my primary supervisor, Professor Jorge Martins, who guided me throughout this project and for his willingness to impart his knowledge, and to Professor André Carvalho, whose support and encouragement allowed my studies to flourish.

Finally, I wish to thank my parents for their love and encouragement, without whom I would never have enjoyed so many opportunities.

Resumo

Esta tese elabora sobre os mecanismos subjacentes de agarrar e de um sistema oscilante. Este Sistema utiliza métodos de controlo por impedância para se estabilizar e alcançar um comportamento cíclico, onde um objeto, uma caneta, é oscilado por dois dedos robóticos.

Um sistema de percepção bio inspirada é empregue para a deteção da posição do objeto, em relação à mão robótica, que por sua vez utiliza esta informação para a sua manipulação. Esta deteção é obtida por via das forças e posição de ditas forças nas pontas dos dedos do sistema robótico.

Pela percepção da posição das pontas dos dedos do sistema, e da anteriormente referida deteção da posição da caneta, um método de controlo de impedância foi apresentado, através do controlo da força de aperto e do seguimento de uma referência sinusoidal para a trajetória do objeto.

Adicionalmente, a análise do sistema permitiu estudar a presença de uma frequência de ressonância à qual a magnitude de oscilação do objeto pode ser maximizada. A resposta do sistema é discutida para uma gama de frequências, amplitudes e deslocamentos da posição inicial da caneta. A frequências mais altas, o fenómeno de duplicação de período é evidente, onde uma nova trajetória periódica emerge de uma trajetória periódica preexistente.

Palavras-Chave: Agarramento bio inspirado, Comportamento cíclico, Controlo de impedância, Impedância em agarrar, Sistema oscilatório.

Abstract

This thesis covers the underlying mechanisms of grasping and an oscillating system. It uses impedance control methods to stabilize the system and reach a cyclical behavior where an object, a pen, is oscillated by two robotic fingers.

A bio-inspired perception system is employed for the detection of the position of the object, in relation to the robotic hand, which in turn uses this information for its manipulation. Such detection is obtained via the forces and position of said forces on the fingertips of the robotic system.

Through the system's perception of the position of its fingertips and the aforementioned detection of the pen's position, an impedance control method was put forward, through the control of the grasping force and the following of a sinusoidal reference for the object's trajectory.

Further, the analysis of the system allowed to study the presence of a resonant frequency at which the oscillation magnitude of the object can be maximized. The system's response is discussed for a range of frequency, amplitude and offset of the pen's position. At higher frequencies, the phenomenon of period doubling is made evident, where a new periodic trajectory emerges from the existing periodic trajectory at which the pen had been moving thus far.

Keywords: Bioinspired grasping, Cyclical behavior, Impedance control, Impedance of grasping, Oscillating system.

Nomenclature

Kinetic Symbols

d	Radius of the fingertip
w	Diameter of the pen
L	Length of the pen
$\boldsymbol{R}_n^m, \dot{\boldsymbol{R}}_n^m$	Rotation matrix between frame n and frame m, and its derivative in time
$\theta, \dot{\theta}$	Angle of rotation of the wrist and its derivative in time
$q, \dot{q}$	Angle of rotation of the pen and its derivative in time
$\alpha, \dot{\alpha}, \ddot{\alpha}$	Angle between finger and pen and its derivatives in time
$r, \dot{r}$	Distance from the wrist to the fingertip and its derivative in time
$\delta, \dot{\delta}$	Penetration distance between pen and finger and its derivative in time
$\dot{\delta}_-$	Penetrating velocity value on impact
s	Distance between finger and pen, x-component
s_x	Distance between finger and pen on the contact point, x-component
$\boldsymbol{c}_1, \dot{\boldsymbol{c}}_1$	Pen's contact point's position and its derivative in time
$\boldsymbol{c}_2, \dot{\boldsymbol{c}}_2$	Finger's contact point's position and its derivative in time
$\boldsymbol{p}_1, \dot{\boldsymbol{p}}_1$	Pen's position and its derivative in time
$\boldsymbol{p}_2, \dot{\boldsymbol{p}}_2$	Finger's position and its derivative in time
$\boldsymbol{\omega}_1$	Pen's angular velocity vector
v_1	Relative velocity of the pen's contact point to the pen
v_2	Relative velocity of the finger's contact point to the finger
v_r	Relative velocity between finger and pen
v_x	Relative velocity of contact points of pen and finger, x-component
λ	Interfinger distance on the pen's body
γ	Height position of the pen
h	Height position of the pen in relation to the fingers
M	Point in the intersection of a line intersecting both fingers' center of mass and the pen's x_1 axis
$\hat{\boldsymbol{r}}_{M,1}$	Distance from point M to center of mass of pen (frame 1)
$\hat{\boldsymbol{r}}_{0,M}$	Distance from frame 0 to point M

Dynamic Symbols

m_p	Mass of the pen
m_f	Mass of the finger
g	Acceleration of gravity
$I_{z,p}$	Inertia of the pen regarding the z-axis, around its center of mass
$I_{z,f}$	Inertia of the finger regarding the z-axis, around its center of mass
$I_z, I_{z,d}$	Inertia of the system and desired inertia of the system regarding the z-axis
F, F_x, F_y	Force and its components
T	Torque
F_n	Normal force
F_t	Friction force
$F_{t,s}$	Static friction force
$F_{t,d}$	Dynamic friction force
K	Stiffness coefficient of the normal force
k	Nonlinear stiffness coefficient of the normal force
ε	Restitution coefficient of the normal force
β	Inverse restitution coefficient of the normal force
a	Geometry coefficient of the normal force
μ_s	Static friction coefficient
μ_d	Dynamic friction coefficient
K_s	Static friction stiffness coefficient
λ	Static friction damping coefficient
η	Static friction damping coefficient
γ	Smoothing coefficient for the static friction
v_{lim}	Velocity threshold for the transition between dynamic to static friction state

Control Symbols

T_s	Time sample
$q_r, \dot{q}_r$	Reference signal for the pen's angle and its derivative in time
A	Amplitude of input reference signal sine wave for the pen's angle
ω	Frequency of input reference signal sine wave for the pen's angle
ω_r	Resonant frequency of the system
$r_r, \dot{r}_r$	Reference for the center point of the fingers and its derivative in time
δ^*	Penetration distance equivalent such that the forces produced in grasping are enough to hold the pen

δ_r	Reference for the penetration distance
q_{max}	Max absolute value for q over the duration of the simulation
θ_{max}	Max absolute value for θ over the duration of the simulation
$K_{p,f}$	Control gain of the position of the center-point of the fingers
$K_{d,f}$	Control gain of the velocity of the center-point of the fingers
$K_{v,f}$	Control gain of the velocity of the fingers
$K_{p,\delta}$	Control gain of the δ
K_T	Control gain of the angle of the object
D_T	Control gain of the angular velocity of the object

List of Figures

Figure 1.1 – Depicted some early humans in the act of tool making.. 1
Figure 2.1 – Pen model 3
Figure 2.2 – Robotic hand model 3
Figure 2.3 - Pen model designed in SolidWorks. 4
Figure 2.4 - Robotic hand model, (…) in SolidWorks. 5
Figure 2.5 – Fingertip in relation to reference frame 0 6
Figure 2.6 - Visualization of the penetrating distance, δ. (1) Pen's body, (2) Finger's body 7
Figure 2.7 – Pen and finger with their corresponding velocities and angular velocities drawn. 9
Figure 2.8 – Normal force varying with the penetration distance, δ, and its velocity, $\dot{\delta}$. 10
Figure 2.9 – State machine of the friction force. 11
Figure 2.10 – Static friction force varying with the displacement sx and tangential velocity vx 13
Figure 3.1 – The four mechanoreceptors responsible for the sense of touch 17
Figure 3.2 – The muscle spindle, ... 19
Figure 4.1 – Pen between the fingers and definition of relevant variables for detection 24
Figure 4.2 – More relevant variables for detection 26
Figure 4.3 – Validation of the estimation of the position of the pen 27
Figure 4.4 – Estimation of the pen's angular acceleration. 28
Figure 4.5 – Estimation of the position of the pen 28
Figure 5.1 – Estimation of the penetration distance δ 32
Figure 5.2 – Block diagram for the control methods employed 34
Figure 5.3 – Controller action 35
Figure 5.4 – Reference signal for the pen's angle and the pen's angle q, side by side 35
Figure 5.5 – Plot of the estimated and real position of the pen 36
Figure 6.1 – Representation of a half-cycle of the pen oscillation movement on the fingers 39
Figure 6.2 – Sequence of frames of the action of oscillating the pen on the fingertips, with the system oscillating at the resonant frequency 40
Figure 6.3 – Sequence of frames of the action of oscillating the pen on the fingertips, with the system oscillating at high frequency 41
Figure 6.4 – Representation of important variables for the simplified system. 42
Figure 6.5 – Response of the system to frequencies ranging from 1 to 60 rad/s. 43
Figure 6.6 – Parametric plot of the pen's angle q and the pen's angular velocity q at frequencies of 4, 12 and 20 rad/s 45
Figure 6.7 – Parametric plot of the pen's angle q and wrist's angle θ at frequencies 4, 12, 20 rad/s. 46
Figure 6.8 – Parametric plot of the pen's angle q and the pen's angular velocity q at frequencies of 46, 52 and 58 rad/s 47
Figure 6.9 – Parametric plot of the pen's angle q and wrist's angle θ, at frequency of 58 rad/s 47
Figure 6.10 – System's response to amplitudes ranging from 0 to 1.25 48
Figure 6.11 - System's response to an offset being introduced in the initial position of the pen 49

List of Tables

Table 1 – Parameters of the dynamic models 4
Table 2 – Normal force parameters 11
Table 3 – Friction force parameters. 12
Table 4 – Cutaneous mechanoreceptor system 19
Table 5 - First twenty terms for the recursion in (2.21) 53

Table of Contents

Acknowledgments ... **ii**

Resumo ... **iv**

Abstract ... **vi**

Nomenclature ... **viii**

List of Figures ... **xii**

List of Tables ... **xiv**

Table of Contents ... **xvi**

1 Introduction ... **1**

1.1 Motivation ... 1

1.2 Objective and Methods ... 2

2 Model ... **3**

2.1 Simulation environment ... 4

2.1.1 Pen ... 4

2.1.2 Hand ... 5

2.2 Contact ... 5

2.2.1 Fingertip position and velocity in the $< xy > 0$ plane ... 5

2.2.2 Object penetration distance ... 6

2.2.3 Contact points' kinematics ... 8

2.2.4 Relative velocity between the finger and pen at the point of contact ... 9

2.2.5 Normal force ... 10

2.2.6 Frictional force ... 11

2.2.6.1 Static friction (Adhesion) ... 12

2.2.6.2 Dynamic friction (Sliding) ... 13

2.2.7 Forces and torque applied on the system ... 14

3 Physiology of the human touch - Perception ... **17**

3.1 Skin mechanoreceptors ... 17

3.1.1 Meissner corpuscles ... 18

3.1.2 Merkel cells ... 18

3.1.3 Pacinian corpuscles ... 18

3.1.4 Ruffini endings ... 18

3.2 Muscle mechanoreceptors ... 19

3.2.1 Muscle spindle ... 19

3.2.2 Golgi tendon organ 20
3.3 Spinal cord 20
3.4 Model variables usable from the model 20

4 Estimation of the pen's position 23
4.1 Angle estimation 23
4.2 Position estimation 23
4.3 Validation 26

5 Controller 31
5.1 Finger position control 31
5.2 Stable grasping impedance 32
5.3 Object manipulation impedance 33
5.4 Block diagram 34
5.5 Analysis and discussion 34
5.6 Analysis and discussion of the pen's estimated position, governed by the controller 36

6 System's response analysis and exploration 39
6.1 Linearized system analysis 42
6.2 Response of the system to frequency 43
6.3 Cyclical behavior analysis: low and resonant frequency 45
6.4 Cyclical behavior analysis: high frequency 46
6.5 Robustness to input amplitude and pen offset 48

7 Conclusions 51
7.1 Achievements 51
7.2 Future work 51

Appendix A 53

References 55

1 Introduction

1.1 Motivation

The act of object grasping is quite a complex ability, unique to some select few in the animal kingdom [1] and without a doubt the most important trait that allowed for the evolution of *Homo sapiens*, humans, as we know them today. It allowed early primates to take up tool use [2] and to control fire [3, 4], two defining abilities that mark the start of the human era.

Grasping is not easy, which is reflected on the abundance, or lack thereof, of this ability in the wild [2]. This technique proves very worthwhile, though the combination of high dexterity and intelligence is often prohibitive to many, it rewards greatly those who master it [5] with a rapid ascension in the food chain hierarchy.

This ability was used by ancient humans for tool making [6, 7] and it took up a big part of their time, where the ability to grasp and work the tool were crucial for survivability. A depiction of such activity is illustrated in Figure 1.1.

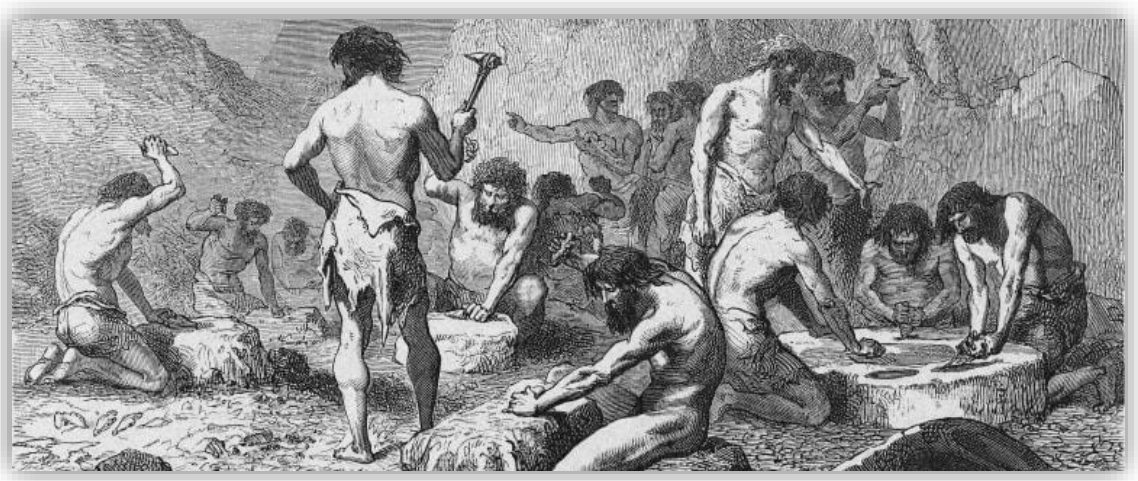

Figure 1.1 – Depicted some early humans in the act of tool making. Tool use can be seen abundantly, marking just how important grasping mastery truly is. Drawn from [8].

The motivation behind this essay lies on the drive to better understand the art of grasping and the ability for complex hand maneuvers. How this knowledge could be applied to robotics or possibly prosthetics, where a mechanical system need be able to execute the fluid yet complex movements a human can do with ease, almost without any critical thinking behind it.

Contemporary uses of grasping in robotic handling generally consist of holding the grasped object steady and firmly to manipulate it [9, 10, 11]. In these cases, the robot does not consider motion decoupled from the object being manipulated.

Some research has also been done on the controlled grasping of fragile items, including catching a falling egg [12] and grabbing a house-hold mug [13]. The former made use of an impedance control strategy to successfully catch falling raw eggs without breaking them.

This work attempts to use the mix of quick movements and impedance control to dynamically manipulate and oscillate an object, and to act as an inspiration for further development in the dynamic manipulation of objects.

1.2 Objective and Methods

The goal of this study is to build a biologically inspired model of a robotic hand and a controller capable of handling a pen through complex motion, specifically the ability to wiggle the pen on the fingertips, making an oscillating cycling motion. The model must reflect its biological counterparts regarding the sensing and the signal propagation of the system. Additionally, the controller should be robust regarding the system's operating characteristics and outside factors that might disturb the well-functioning of the system.

Towards this goal, such model was constructed, and an impedance-based control was implemented at the level of grasping and object maneuverability, while position control was implemented at the level of the positioning of the fingers. The system's response is then thoroughly discussed and analyzed so as to evaluate its stability, robustness and cyclicity.

2 Model

The geometric hypotheses for the model are that the problem can be simplified as a 2-D task, both fingertips are of circular geometry, the pen is cylindrical and perfectly straight, and the contact occurs in a singular point on the bodies. Given these, a kinematic model for each body was created. For ease of writing, the pen will be referenced as body 1 and the upper fingertip and lower fingertip as body 2 and $2'$ respectively in this document. Below, in Figure 2.1, the pen's model is illustrated. In Figure 2.2 the robotic hand's model is illustrated, where its construction is displayed.

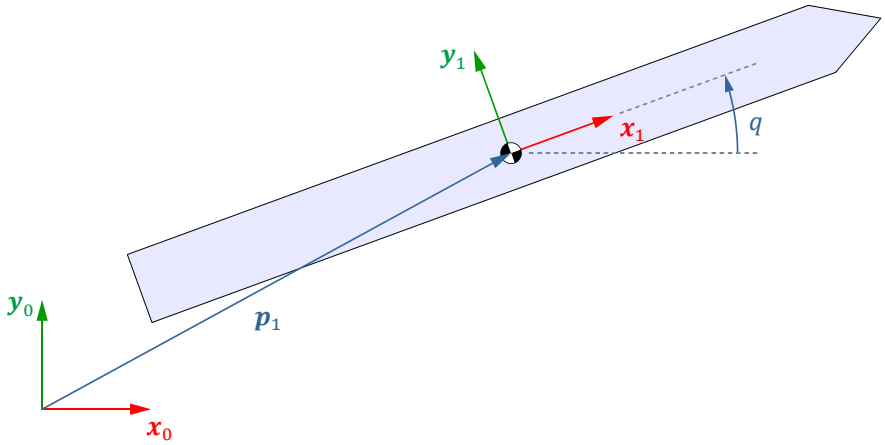

Figure 2.1 – Pen model. The pen is able to move along both the x-axis and y-axis and is able to rotate around the z-axis and its rotation is given by the angle q. Its reference frame is numerated with the number 1.

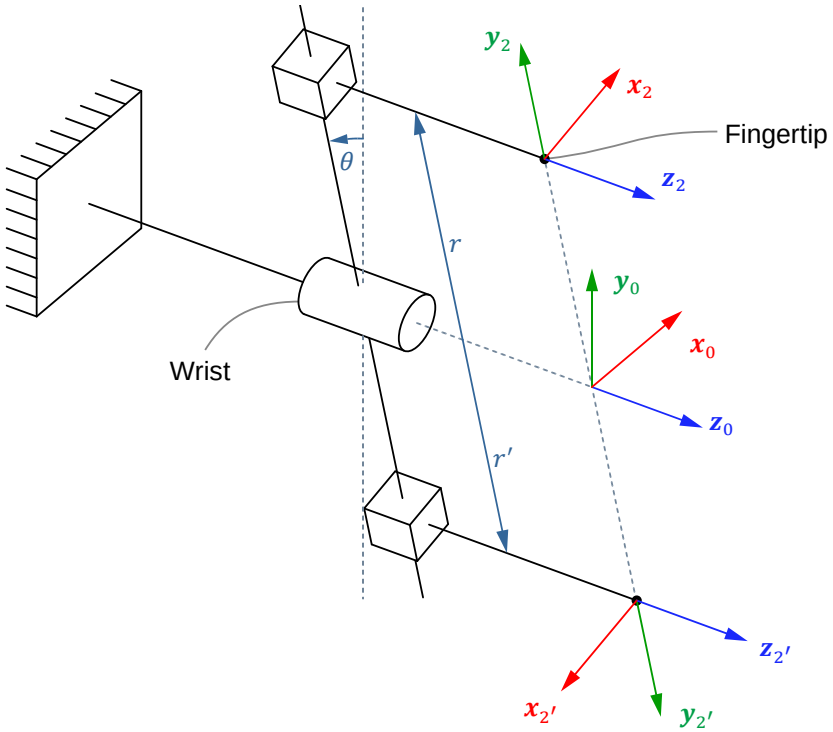

Figure 2.2 – Robotic hand model. The wrist joint is represented as a cylinder, conveying a rotation between the fixed base and the fingertips by an angle θ. The fingertips have their respective frames of reference attached to them, namely 2 and $2'$. Their displacement from the rotation axis, z_0, is measured along y_2 and y_2', as noted by r and r'.

The hypotheses in relation to the contact are that the bodies have a constant friction coefficient between the surfaces (fingertip-pen) and that there are no adhesive forces. The model used for the normal contact forces was the Hunt-Crossley model, with a non-adhesive exponential extension [14]. For the tangential forces, an adaptation of the static-kinetic friction by Coulomb [15] is used. Both will be detailed further ahead into the document.

The dynamic model was formulated in Simscape™, a modeling tool within the Simulink® environment. This modeling tool was chosen as it facilitates a high-performance formulation for the dynamics of the multibody system, whose parameters are gathered in Table 1. Through this approach, the user need only specify the forces affecting each body and the motion constraints between them.

Towards this end, a construction that follows the aforementioned models was designed in SolidWorks, in order to be used in Simscape™ to visualize the bodies in motion. The construction of the two bodies is detailed in the next section.

Table 1 – Parameters of the dynamic models. The finger corresponds to the full finger, including the fingertip and the finger body, moved by the prismatic joint. The inertia that of the body's z-axis, at its center of mass. The center of mass is in relation to the geometric center of the object, in the 2-D plane considered in this document.

	Mass $[g]$	Inertia (z-axis) $[g\ mm^2]$	Center of mass $[mm]$
Pen	4.5	7099.9	$[0 \quad 0 \quad 0]^T$
Finger	16.3	1651.7	$[0 \quad 0 \quad 55.55]^T$
Base	158.7	17584.0	$[0 \quad 0 \quad 0]^T$

2.1 Simulation environment

The environment consists of the two subsystems, the robotic hand and the pen. These are simulated in a virtual world that is affected by gravity, with a magnitude of $9.81\ \mathrm{m/s^2}$ and the negative direction of the y-axis.

2.1.1 Pen

The pen, modeled in SolidWorks, is cylindrical and perfectly straight. Its center of mass is located at its geometric center. It has a length of 132 mm and a diameter of 8 mm, illustrated in Figure 2.3.

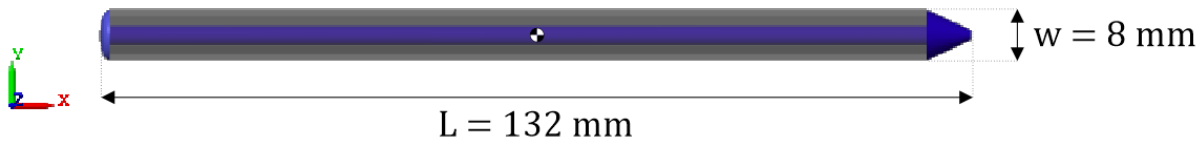

Figure 2.3 - Pen model designed in SolidWorks, with its respective dimensions and frame of reference.

2.1.2 Hand

The robotic hand also had its wrist modeled in SolidWorks, while its the fingers were adapted from another source [16]. The fingertips are identical and cylindrical, with a radius of 8.89 mm. The full robotic hand construction is illustrated in Figure 2.4.

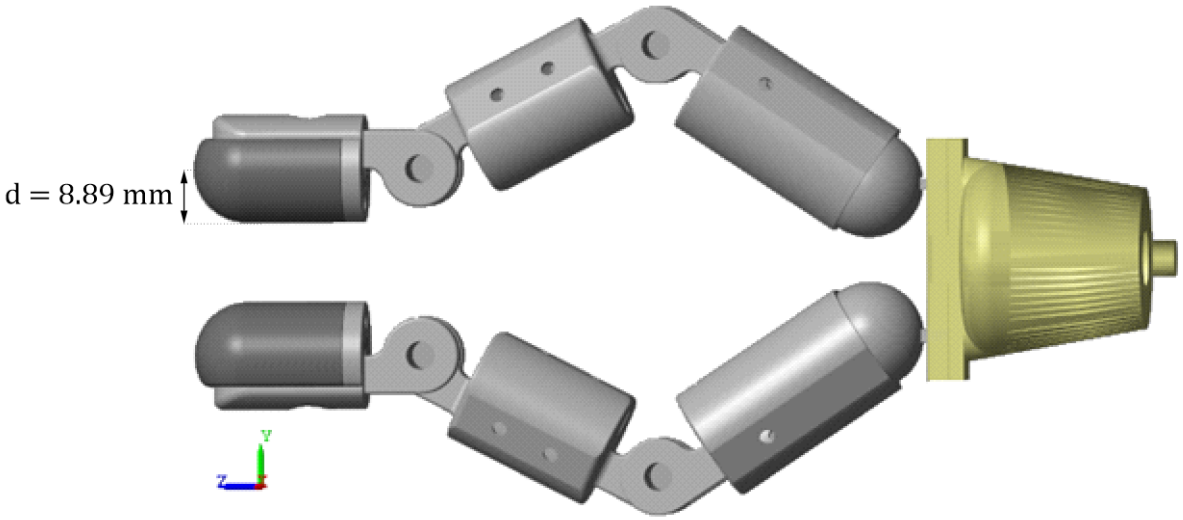

Figure 2.4 - Robotic hand model, wrist (in yellow) designed in SolidWorks and fingers (in grey) adapted from [16], with its respective frame of reference.

2.2 Contact

By using the position and velocity of the pen and fingertips it is possible to obtain the forces that would result from the contact between them. These forces are then applied to these entities to simulate their motion. In the next calculations, the equations presented refer to the interaction between the upper fingertip and the pen. The dynamics for the lower fingertip will be equivalent, often symmetrical to those of the upper finger.

2.2.1 Fingertip position and velocity in the $< \mathrm{xy} >_0$ plane

Using simple trigonometry, the finger's position and velocity in the world frame of reference is calculated. This is clear in Figure 2.5 and is followed up with equation (2.1).

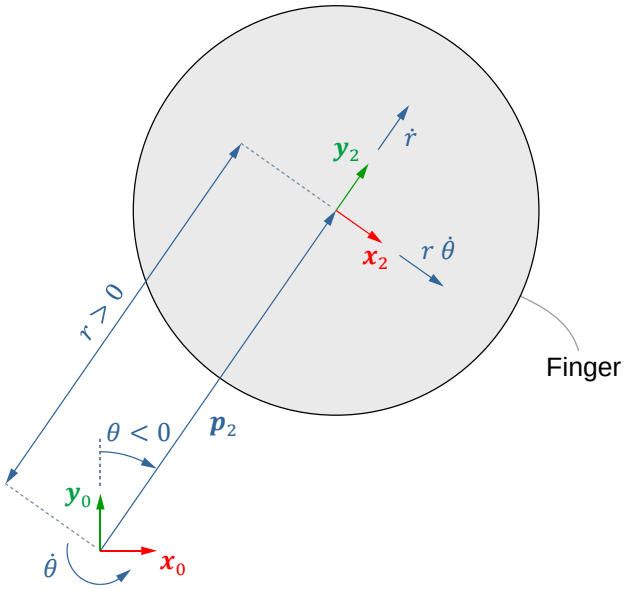

Figure 2.5 – Fingertip in relation to reference frame 0 (world frame). The variables that describe its motion are the distance to the wrist r, and the wrist's angle of rotation θ.

$$\boldsymbol{p_2} = \begin{bmatrix} -r\sin(\theta) \\ r\cos(\theta) \\ 0 \end{bmatrix},\ \dot{\boldsymbol{p}}_2 = \begin{bmatrix} -\dot{r}\sin(\theta) - r\cos(\theta)\,\dot{\theta} \\ \dot{r}\cos(\theta) - r\sin(\theta)\,\dot{\theta} \\ 0 \end{bmatrix} \tag{2.1}$$

2.2.2 Object penetration distance

To define a contact event between the finger and the pen, the distance between the finger and the pen needs to be determined. In this case, the distance of penetration (δ) is calculated instead, where it is positive $(\delta > 0)$ if the bodies are penetrating each other, meaning contact is taking place, or non-positive $(\delta \leq 0)$ if they are apart [14]. In other words, it is considered that

$$\text{the finger and the pen are } \begin{cases} \text{separated}, & \text{if } \delta \leq 0, \\ \text{in contact}, & \text{if } \delta > 0. \end{cases} \tag{2.2}$$

Analyzing Figure 2.6 it is clear that δ, d and $w/2$ relate to the positions of the bodies, specifically to their y component on reference frame 1 (the pen). Since there is a need to rotate between reference frames around the z-axis (2-D), rotation matrices will be used throughout the document, denoted as $\boldsymbol{R}$. To rotate the vector components from reference frame 1 to reference frame 0, the respective rotation matrix is

$$\boldsymbol{R}_z(q) = \boldsymbol{R}_1^0 = \begin{bmatrix} cos(q) & -\sin(q) & 0 \\ \sin(q) & \cos(q) & 0 \\ 0 & 0 & 1 \end{bmatrix}, \tag{2.3}$$

while the rotation matrix to rotate back to reference frame 1, from reference frame 0, is simply the transpose of this matrix, $\boldsymbol{R}_1^{0^T} = \boldsymbol{R}_0^1$. Furthermore, for simplicity, the rotation $\boldsymbol{R}_1^0$ is often denoted as $\boldsymbol{R}_1$.

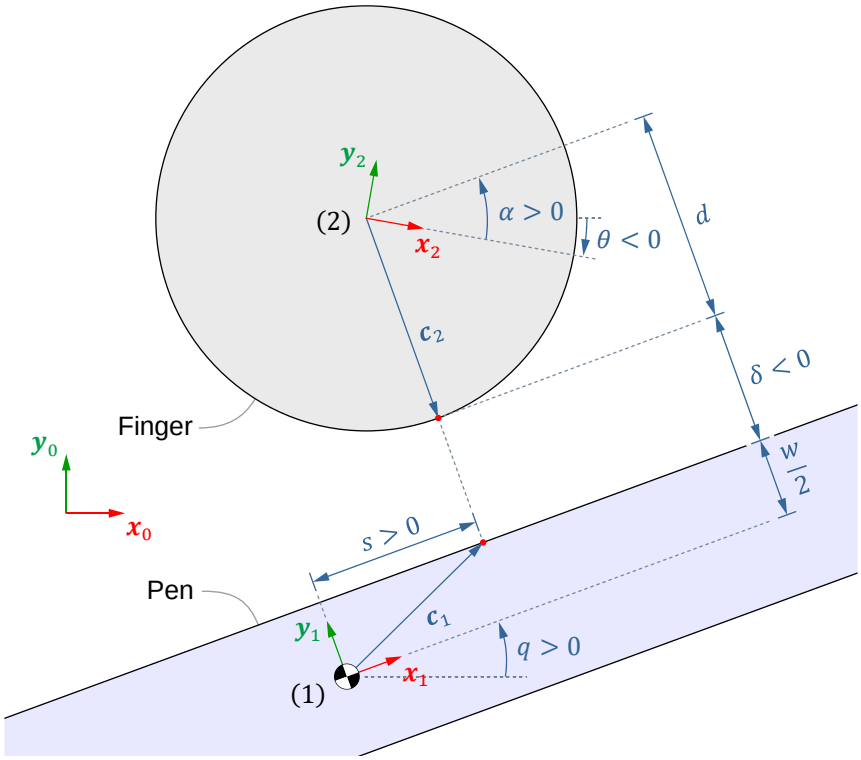

Figure 2.6 - Visualization of the penetrating distance, δ. (1) Pen's body, (2) Finger's body. The point in each body that is the closest to the other body is drawn in red. The position vector of the contact points of the pen and the fingertip, c_1 and c_2 respectively are also drawn. The angle α relates the rotation between reference frame 1 and reference frame 2.

The relative displacement between the bodies' positions, $\boldsymbol{p}_2 - \boldsymbol{p}_1$, may be projected onto the y-axis of the pen's frame through $\hat{\boldsymbol{j}}^T \boldsymbol{R}_1^T(\boldsymbol{p}_2 - \boldsymbol{p}_1)$. This distance is equal to negative δ plus the thickness of the bodies, or

$$\hat{\boldsymbol{j}}^T \boldsymbol{R}_1^T(\boldsymbol{p}_2 - \boldsymbol{p}_1) = d - \delta + \frac{w}{2}, \tag{2.4}$$

where $\hat{\boldsymbol{j}}$ is the unit vector regarding to the second component. It becomes relevant to define the unit vectors, $\hat{\boldsymbol{\imath}}, \hat{\boldsymbol{\jmath}}, \hat{\boldsymbol{k}}$ as

$$\begin{bmatrix} \hat{\boldsymbol{\imath}} \\ \hat{\boldsymbol{\jmath}} \\ \hat{\boldsymbol{k}} \end{bmatrix} = \begin{bmatrix} 1 & 0 & 0 \\ 0 & 1 & 0 \\ 0 & 0 & 1 \end{bmatrix}. \tag{2.5}$$

From equation (2.4), the penetrating distance is readily obtained as

$$\delta = d + \tfrac{w}{2} - \hat{\boldsymbol{j}}^T \boldsymbol{R}_1^T(\boldsymbol{p}_2 - \boldsymbol{p}_1). \tag{2.6}$$

Furthermore, the velocity of the penetrating distance can be calculated by differentiation of the above equation (2.6), resulting in

$$\dot{\delta} = -\hat{\boldsymbol{j}}^T \left[\boldsymbol{R}_1^T(\dot{\boldsymbol{p}}_2 - \dot{\boldsymbol{p}}_1) + \dot{\boldsymbol{R}}_1^T(\boldsymbol{p}_2 - \boldsymbol{p}_1)\right], \tag{2.7}$$

where $\dot{\boldsymbol{R}}_1^T$ is the time derivative of the rotation matrix $\boldsymbol{R}_1^T$, obtained through $\dot{\boldsymbol{R}} = \frac{\partial \boldsymbol{R}}{\partial q}\dot{q}$, resulting in

$$\dot{\boldsymbol{R}}_1^T = \begin{bmatrix} -\sin(q) & -\cos(q) & 0 \\ \cos(q) & -\sin(q) & 0 \\ 0 & 0 & 0 \end{bmatrix}^T \dot{q}. \tag{2.8}$$

2.2.3 Contact points' kinematics

The point in each body that is the closest to the other body are now determined. Each one is expressed in the reference frame of the body they belong to. Recalling Figure 2.6, $\boldsymbol{c}_1$ is obtained from the sum of its vectorial components s and $w/2$. Similarly, to δ in equation (2.6), s is calculated as

$$s = \hat{\boldsymbol{\imath}}^T \boldsymbol{R}_1^T (\boldsymbol{p}_2 - \boldsymbol{p}_1), \tag{2.9}$$

where $\hat{\boldsymbol{\imath}}$ is the unit vector regarding to the first component. Thus, the position vector for the contact point on the pen can be written as

$$\boldsymbol{c}_1 = [s \quad w/2 \quad 0]^T. \tag{2.10}$$

Moving on to the contact point on the finger $\boldsymbol{c}_2$, when expressed in the pen's reference frame (frame 1), it is simply its radius in the direction normal to the pen, therefore it is

$$\boldsymbol{R}_2^1 \boldsymbol{c}_2 = [0 \quad -d \quad 0]^T, \tag{2.11}$$

where $\boldsymbol{R}_2^1$ is the rotation matrix from frame 2 to frame 1, corresponding to a rotation by an angle α, represented in Figure 2.6 as the angle between the fingertip and the pen. The rotation matrix is therefore

$$\boldsymbol{R}_2^{1\,T} = \boldsymbol{R}_1^2 \triangleq \boldsymbol{R}_z(\alpha), \tag{2.12}$$

and the contact point can then be expressed in the finger's reference frame through

$$\boldsymbol{c}_2 = \boldsymbol{R}_1^2 [0 \quad -d \quad 0]^T. \tag{2.13}$$

Finally, the angle α is obtained from the rotation angle between frames 1 and 2. As such, it can be obtained from the rotation angle of frame 1, q, and the rotation angle of frame 2, θ. Thus, from inspection of Figure 2.6, α follows as

$$\alpha = q - \theta, \tag{2.14}$$

and its derivative, $\dot{\alpha}$, is simply

$$\dot{\alpha} = \dot{q} - \dot{\theta}. \tag{2.15}$$

2.2.4 Relative velocity between the finger and pen at the point of contact

The relative velocity between the objects at their collision point can be calculated by the difference of each of the object's contact points' velocities. It then becomes important to know these points' velocities, illustrated in Figure 2.7.

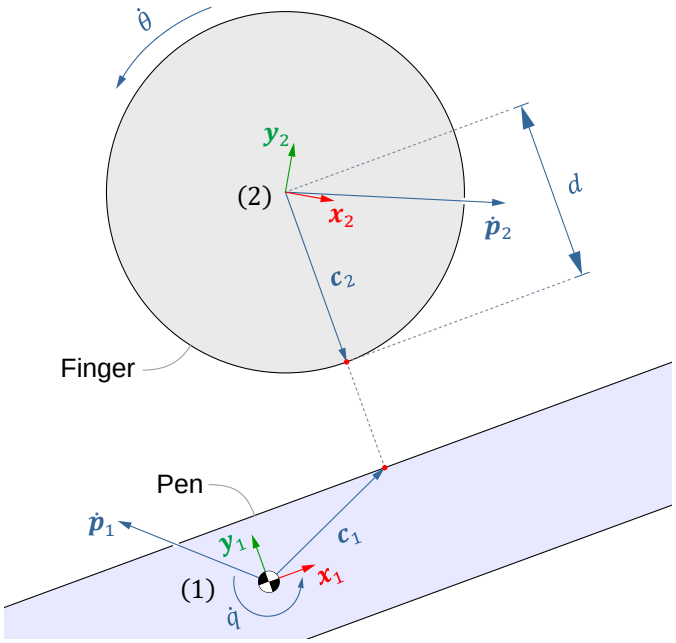

Figure 2.7 – Pen and finger with their corresponding velocities and angular velocities drawn, as well as important dimensions. The point in each body that is the closest to the other body is drawn in red.

The finger's contact point's velocity is then calculated as the sum of the finger's own velocity and the tangential velocity resulting from the angular velocity of the finger and the radius of contact. The finger was considered to be deformable and thus the radius of contact is given as the finger's radius minus the penetration distance δ. The finger's contact point's velocity is then

$$\boldsymbol{R}_2^1\,\boldsymbol{v}_2 = \boldsymbol{R}_0^1\,\dot{\boldsymbol{p}}_2 + \begin{bmatrix} (d-\delta)\dot{\theta} \\ 0 \\ 0 \end{bmatrix}. \tag{2.16}$$

Following the same logic, the pen's contact point's velocity can also be calculated as the sum of the pen's velocity and the tangential velocity resulting from its angular velocity, $\boldsymbol{\omega}_1 = \dot{q}\,\hat{\boldsymbol{k}}$, and the distance between its contact point and the center of mass

$$\boldsymbol{v}_1 = \boldsymbol{R}_0^1\,\dot{\boldsymbol{p}}_1 + \boldsymbol{\omega}_1 \times \boldsymbol{c}_1. \tag{2.17}$$

Lastly, the relative velocity is calculated by subtracting the velocities between the contact points of the objects in equations (2.16) and (2.17), resulting in

$$\boldsymbol{v}_r = \boldsymbol{R}_2^1\,\boldsymbol{v}_2 - \boldsymbol{v}_1. \tag{2.18}$$

2.2.5 Normal force

For the calculation of the normal force between both objects on the event of a collision, the Hunt-Crossley model was used. Furthermore, a non-adhesive extension to this model is implemented, as detailed in [14]. The normal force F_n is given by

$$F_n = \begin{cases} -K\,\delta^a, & \delta \geq 0 \\ 0, & \text{otherwise} \end{cases} \tag{2.19}$$

where a is a geometry exponent and K can be calculated by the expression

$$K = \begin{cases} k\left(1 + \dfrac{\dot{\delta}}{\dot{\delta}_-}\beta\right), & \dot{\delta} \geq -\varepsilon\dot{\delta}_- \\ k(1-\beta\varepsilon)\exp\left(\dfrac{\beta}{1-\beta\varepsilon}\dfrac{\dot{\delta}+\varepsilon\dot{\delta}_-}{\dot{\delta}_-}\right), & \text{otherwise} \end{cases} \tag{2.20}$$

where k is the nonlinear stiffness coefficient of the collision, $\dot{\delta}_-$ is the value of $\dot{\delta}$ right before impact, ε is the restitution coefficient and β is the inverse restitution, given in [14] as

$$\beta = \sum_{n=1}^{\infty} \frac{A_n}{B_n}(\varepsilon - 1)^n \approx -\frac{3}{2}(\varepsilon - 1)\frac{11-\varepsilon}{1+9\varepsilon} \tag{2.21}$$

where the terms A_n and B_n can be found in Table 5 (appendix). The first 20 terms of A_n and B_n were used for the calculation of β. The previous parameters are gathered in Table 2.

An illustration of how the normal force varies with δ and $\dot{\delta}$ is pictured in Figure 2.8, below.

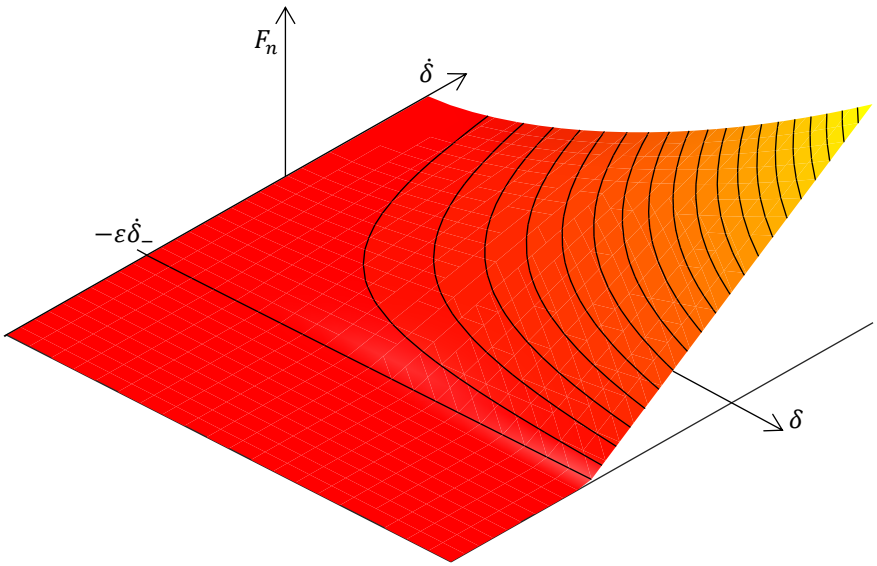

Figure 2.8 – Normal force varying with the penetration distance, δ, and its velocity, $\dot{\delta}$.

Table 2 – Normal force parameters

Parameter	Value	Units
a	$3/2$	$-$
k	2×10^5	N/m^{α}
ε	0.2	$-$
β	4.8719	$-$

2.2.6 Frictional force

The force created by the existence of friction between the two objects can be split into two states, the static friction state, when the objects are in adhesion, and the dynamic friction state, when the objects slide over one another. The transition between these states is detailed in Figure 2.9 and described as follows. This system was adapted from [17].

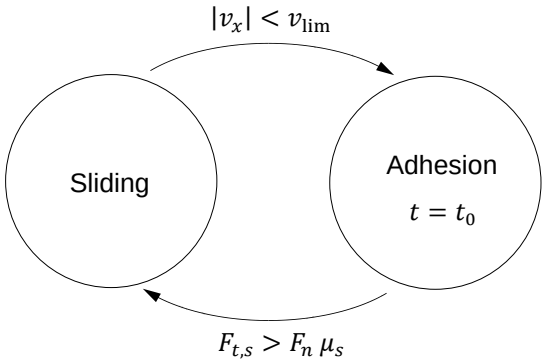

Figure 2.9 – State machine of the friction force. The system begins at the sliding state.

The contact transitions to adhesion if the tangential velocity between the bodies, v_x, is lower than some limit v_{lim}. The transition from adhesion to sliding occurs when the normal force, F_n, multiplied by the static coefficient μ_s is lower than the static friction force $F_{t,s}$.

The sign function is now introduced, as it is relevant for the calculation of the friction forces. It takes in one argument and indicates whether its argument is positive or negative, returning the unit value with its respective sign. This function is defined as

$$\operatorname{sign}(u) = \begin{cases} 1, & u > 0, \\ 0, & u = 0, \\ -1, & u < 0. \end{cases} \tag{2.22}$$

2.2.6.1 Static friction (Adhesion)

In the aforementioned system, the static friction may be modeled as a nonlinear spring that connects and promotes an adhesive force between two bodies. This force is usually written in the form of [17]

$$F_{t,s}^{*} = -K_s s_x \left(1 + \frac{\lambda}{K_s}\text{sign}(s_x)v_x\right), \tag{2.23}$$

compromising a linear spring, with stiffness K_s, and a nonlinear damping, proportional to $\lambda\, s_x$, where s_x is the spring's displacement.

This model presents some drawbacks which are improved upon in this work. The first handicap follows from observation of the force changes around $s_x = 0$. In particular, one finds that the partial derivatives with respect to s_x equate to

$$\lim_{s_x \to 0^-} \frac{\partial F_{t,s}^{*}}{\partial s_x} = -k + \lambda\, v_x \neq \lim_{s_x \to 0^+} \frac{\partial F_{t,s}^{*}}{\partial s_x} = -k - \lambda\, v_x. \tag{2.24}$$

Since the derivatives from below and above are distinct, it is true that the force model in (2.23) is not smooth. That said, in the advent of external forcing terms, the previous non-differentiability may lead to force changes that are nearly discontinuous. Thus, with the goal of unburdening the simulation with an unnecessary stiff behavior, the sign function can be replaced with a sigmoid function, the hyperbolic tangent. In this way, the force is smooth throughout the range of s_x. A smoothing coefficient, γ, is used to tune the logistic function's response, where a smaller γ equates to a smoother transition and a larger one approaches the sign function, $\lim_{\gamma \to \infty} \tanh(\gamma\, x) = \text{sign}(x)$.

Another observation can be found in the fact that $F_{t,s}^{*}$ is not strictly adhesive, in contradiction to the definition of this force. To see this, consider $s_x > 0$ without any loss in generalization, in which case the model should generate and adhesive force, or $F_{t,s}^{*} < 0$. However, when $v_x < -k/\lambda$ it is true that $F_{t,s}^{*} > 0$, which is a separation force. Following [14], this can be solved by the introduction of a stiffness term that increases exponentially with the velocity, $K(\dot{x}) = k\, e^{\eta\, \dot{x}}$, which can be paired with the previous modification to write a differentiable and strictly adhesive friction force as

$$F_{t,s} = -K_s\, s_x \exp(\eta \tanh(\gamma\, s_x)\, v_x). \tag{2.25}$$

Table 3 – Friction force parameters. μ_s adapted from [18] and μ_d from [19].

Parameter	Value	Units
K_s	10^4	N/m^2
η	2×10^4	s/m
γ	80	–
μ_s	0.7	–
v_{lim}	10^{-3}	m/s
μ_d	0.3	–

Here, the spring's displacement, s_x, is calculated from the object's relative tangential velocity by integration,

$$s_x(t) = \int_{t_0}^{t} v_x(u)du + s_x(t_0), \tag{2.26}$$

where t_0 is the time at which the contact is deemed adhesive, seen in Figure 2.9 as the transition from sliding to adhesion, and $t > t_0$ the time during the contact event. Also, $s_x(t_0)$ is the initial spring's displacement from the transition of dynamic to static friction, which will be later calculated in the dynamic friction section, in equation (2.31). Figure 2.10 illustrates how the force varies with the displacement (s_x) and the tangential velocity (v_x).

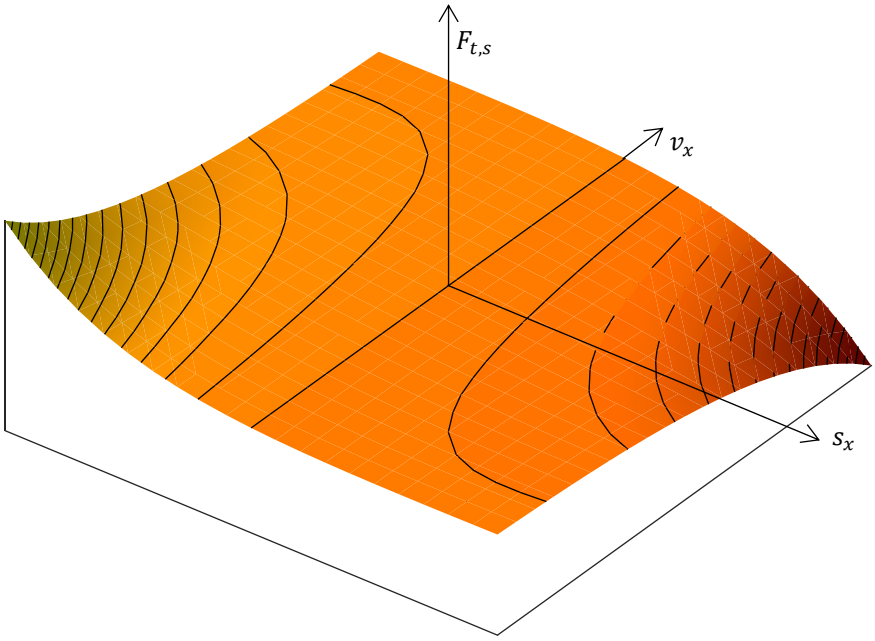

Figure 2.10 – Static friction force, $F_{t,s}$, varying with the displacement s_x and tangential velocity v_x.

Finally, the transition from static to dynamic friction was modeled to occur when the static friction force overcame the allowable force as per Coulomb's friction law [15]. This event happens when

$$F_n\,\mu_s < F_{t,s}, \tag{2.27}$$

where μ_s is the static friction coefficient [18].

2.2.6.2 Dynamic friction (Sliding)

The dynamic friction was also modeled following Coulomb's friction law [15], such that the friction force is given as

$$F_{t,d} = -\text{sign}(v_x)\,F_n\,\mu_d, \tag{2.28}$$

where, once again, v_x is the relative tangential velocity between the finger and the pen and μ_d is the dynamic friction coefficient.

The transition from dynamic friction back to static friction was modeled to happen when the relative tangential velocity between both objects is very small [17, 15], such that

$$|v_x| - v_{\text{lim}} < 0, \tag{2.29}$$

where v_{lim} is a velocity limit that at which the contact is said to be in sliding.

Lastly, to promote a smooth transition from the sliding to the adhesion state, the initial displacement for the spring needs to be calculated. For this to happen, $s_x(t_0)$ is calculated by establishing continuity between the sliding and friction forces, $F_{t,s} = F_{t,d}$. Thus, it is desired to find $s_x(t_0)$ that satisfies

$$K_s\, s_x \exp(\eta \tanh(\gamma\, s_x) v_x) = F_{t,d}. \tag{2.30}$$

As v_x is bound to be very small in value ($v_x \sim 10^{-3}$) from equation (2.29), it is reasonable to state that $\exp(\eta \tanh(\gamma\, s_x) v_{\text{lim}}) \approx 1$. Thus, calculating the initial displacement for the transition yields

$$s_x(t_0) = \frac{F_{t,d}}{K_s}. \tag{2.31}$$

2.2.7 Forces and torque applied on the system

Returning to the hand and the pen models, with all the relevant forces calculated, their impact on the pen can then be summarized as a force from the upper finger,

$$\boldsymbol{F}_1 = \begin{bmatrix} F_t \\ -F_n \\ 0 \end{bmatrix}, \tag{2.32}$$

and lower finger,

$$\boldsymbol{F}'_1 = \begin{bmatrix} F'_t \\ F'_n \\ 0 \end{bmatrix}, \tag{2.33}$$

and a torque

$$T_1 = \widehat{\boldsymbol{k}}^T (\boldsymbol{c}_1 \times \boldsymbol{F}_1 + \boldsymbol{c}'_1 \times \boldsymbol{F}'_1) \tag{2.34}$$

applied on the center of mass of the pen, where $\widehat{\boldsymbol{k}}^T$ is the unit vector regarding the z-axis.

Naturally, following Newton's third law, the force applied on the finger will be of equal magnitude and opposite direction of the force applied on the pen. Furthermore, given the circular geometry of the finger and the arrangement of the joints (Figure 2.2), only the x component of the force applied on it produces a torque about z_0. That said, the force being acted on the upper finger is

$$\boldsymbol{F}_2 = \boldsymbol{R}_1^2(-\boldsymbol{F}_1), \tag{2.35}$$

and on the lower finger is

$$\boldsymbol{F}'_2 = \boldsymbol{R}_1^{2'}(-\boldsymbol{F}'_1), \tag{2.36}$$

thus, the torque follows from the distance between the finger's rotation joint, the wrist, and the point of contact, and the force applied on the point of contact, resulting in

$$T_2 = -\hat{\boldsymbol{\imath}}^T \boldsymbol{F_2}(r - (d - \delta)) - \hat{\boldsymbol{\imath}}^T \boldsymbol{F'_2}(r' - (d - \delta')). \tag{2.37}$$

Note that T_2 is exerted about z_0 of the revolute join, while F_2 is exerted along y_2 of the prismatic joint and F'_2 along y'_2.

3 Physiology of the human touch - Perception

With the purpose of creating a bio-inspired controller for the hand, it is important for the perception of the model to also be nature-like and to follow the physiological limits of a human hand. It therefore is essential to know the intricacies of the human touch, which means getting to know the mechanoreceptors in the fingertips and in the relevant muscles, in order to replicate their behavior.

3.1 Skin mechanoreceptors

A mechanoreceptor is a sensory receptor that responds to mechanical pressure or distortion. There are several types of these sensors within the human skin. This document focuses on the study of the mechanoreceptors located in glabrous (hairless) mammalian skin, which is the skin present in the fingertips of primates and other mammals similar to humans. There are four main types of mechanoreceptors in the skin region, namely Meissner corpuscles, Merkel cells, Pacinian corpuscles and Ruffini endings. A summarized description of these can be found in Table 4, taken from [20].

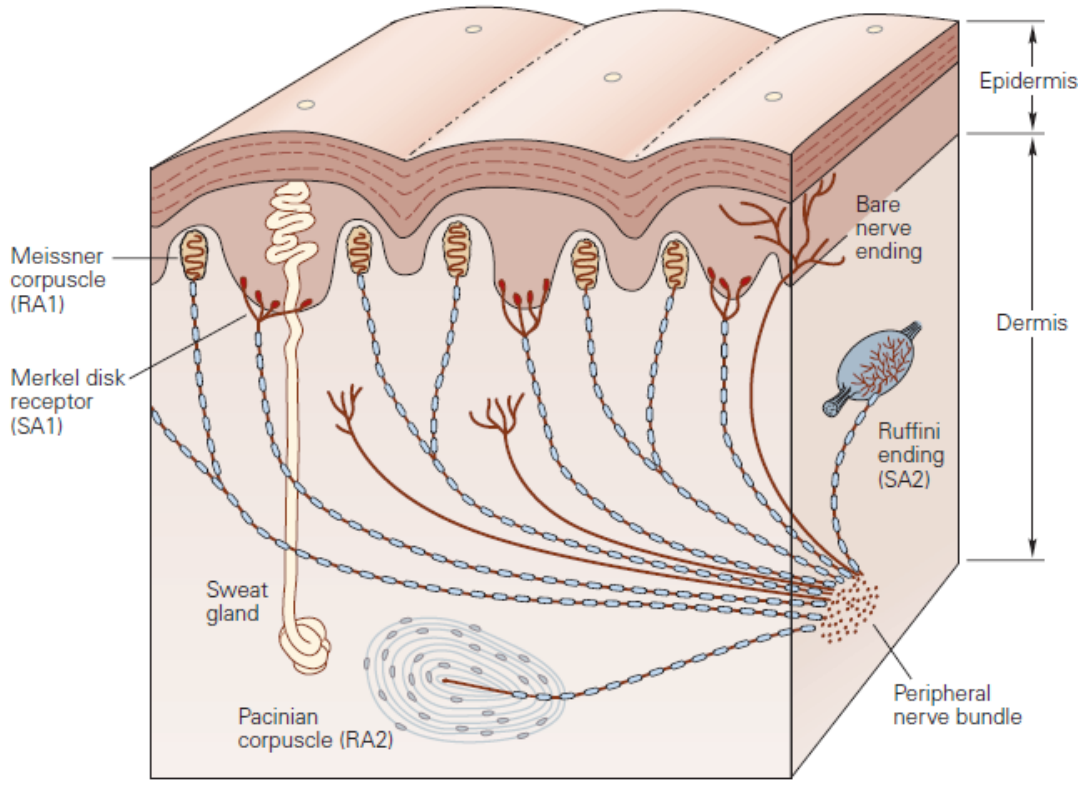

Figure 3.1 – The four mechanoreceptors responsible for the sense of touch, illustrated in the cross section of the glabrous skin shows the principal receptors for touch. The Meissner corpuscles and Merkel cells lie in the superficial layers of the skin, 0.5 to 1.0 mm below the skin surface. The Pacinian and Ruffini corpuscles lie within the dermis, 2-3 mm below the skin surface. This figure was taken from [20].

3.1.1 Meissner corpuscles

The Meissner corpuscle is a rapid adapting type 1 (close to skin surface) receptor, abbreviated as RA1. This receptor is illustrated near the epidermis on Figure 3.1. This corpuscle is responsible for sensitivity to light touch, slippage of objects and the detection of the texture of surfaces it encounters. In particular, they have their highest sensitivity when sensing vibrations between 10 and 50 hertz. The key features that the Meissner corpuscle would be able to integrate into the present model are then:

- Normal force;
- Tangential force.

3.1.2 Merkel cells

Merkel cells are slowly adapting type 1 receptors, abbreviated as SA1, located near the epidermis, as visualized in Figure 3.1. They are responsible for detecting the amount of pressure applied on the skin and are particularly sensitive to edges, corners and points. Similarly to the Meissner corpuscle, they also play an important role in the detection of textures. The key features that the Merkel cells would be able to integrate into the present model are then:

- Position of contact with the finger and its rate of change.

3.1.3 Pacinian corpuscles

The Pacinian corpuscle is a rapid adapting type 2 (deep in the skin) receptor, abbreviated as RA2, which is located in the subcutaneous tissues (dermis). They can be identified in Figure 3.1 deep within the dermis. This mechanoreceptor is larger than the others and is responsible for the detection of higher frequency vibrations, ranging from 5 to 1000 hertz. The detection of vibrations has no impact in the development of this model and as such this corpuscle does not provide any meaningful information.

3.1.4 Ruffini endings

Ruffini endings are slowly adapting type 2 receptors, SA2, that extend from the subcutaneous tissue to folds in the skin at the joints, in the palm or in the fingernails. These receptors are sensitive to the shape of large objects and can signal movements of the fingers and other joints due to stretch in the overlying skin. In combination with the muscle mechanoreceptors, mentioned in the next section, the key features that the Ruffini endings would be able to integrate into the present model are then:

- Position of finger;
- Position of the wrist.

Table 4 – Cutaneous mechanoreceptor system, as found in [20].

	Type 1		Type 2	
	SA1	**RA1**[1]	**SA2**	**RA2**[2]
Receptor	Merkel cell	Meissner corpuscle	Ruffini ending	Pacinian corpuscle
Location	Tip of epidermal sweat ridges	Dermal papillae (close to skin surface)	Dermis	Dermis (deep tissue)
Axon diameter (μm)	7–11	6–12	6–12	6–12
Conduction velocity (ms)	40–65	35–70	35–70	35–70
Best stimulus	Edges, points	Lateral motion	Skin stretch	Vibration
Response to sustained indentation	Sustained with slow adaptation	None	Sustained with slow adaptation	None
Frequency range (Hz)	0–100	1–300		5–1,000
Best frequency (Hz)	5	50		200
Threshold for rapid indentation or vibration (best) (μm)	8	2	40	0.01

[1]Also called RA, QA, or FA1.
[2]Also called PC or FA2.
RA1, rapidly adapting type 1; **RA2**, rapidly adapting type 2; **SA1**, slowly adapting type 1; **SA2**, slowly adapting type 2.

3.2 Muscle mechanoreceptors

3.2.1 Muscle spindle

Muscle spindles are proprioceptors whose main function it is to provide information on muscle length and the rate of change of muscle length. These receptors run parallel to the muscle fibers and are composed of three main parts: (1) Intrafusal muscle fibers; (2) sensory fibers that terminate in the noncontractile regions of the intrafusal fibers; and (3) motor axons that terminate in the contractile regions of the intrafusal fibers, as illustrated in Figure 3.2.

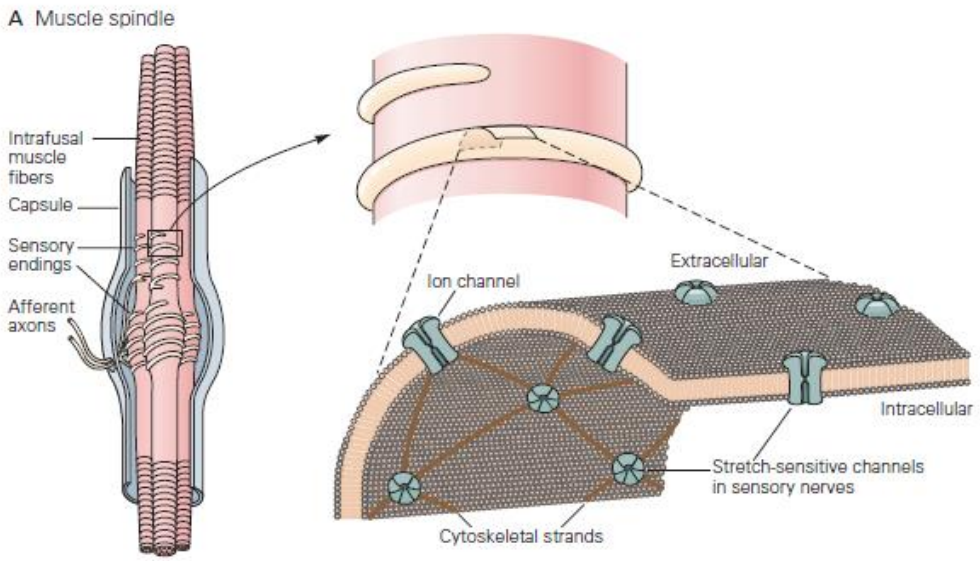

Figure 3.2 – The muscle spindle, the principal receptor mediating proprioception. Its three main components, are: (1) Intrafusal muscle fibers; (2) Sensory endings; and (3) Afferent axons. This figure was taken from [20].

The key features that the muscle spindle would detect from the model are then:

- Position and velocity of the finger;
- Angle and angular velocity of the wrist.

3.2.2 Golgi tendon organ

The Golgi tendon organ is a proprioceptor located at the junction between skeletal muscles and tendons. It is a slender encapsulated structure that has as its main function to detect muscle force.

This organ does not provide meaningful information for the model at hand as the forces affecting the muscles are not used for the control of the task.

3.3 Spinal cord

To convey the somatosensory information acquired by the mechanoreceptors $A\alpha$ nerve fibers stretch from the nerve bundles where the receptors are connected, through the spinal cord to the brain for decision making. The nerve fiber distance between the fingertip and the brain is approximately 0.8 meters [20] and its conduction velocity is 35-70 m/s (Table 4), meaning that in $A\alpha$ nerve fibers delays range 7.5 milliseconds to 12.5 milliseconds, with the mean delay being 10 milliseconds and the arrival times varying by only 5 milliseconds [20].

Furthermore, in voluntary movement, “movement-related (neural) activity typically begins 50 to 150 ms before the onset of agonist muscle activity”, found in [20].

There are then two types of delay in the neurological system, an inbound delay of about 10 milliseconds, that affects perception, and an outbound delay of about 100 milliseconds, that affects the action response.

3.4 Model variables usable from the model

It then follows that from the many sensory cells and mechanisms discussed above that there are a total of 14 state variables usable for the perception and control of the pen. Briefly, these are:

1. Angle between the pen and the upper finger $(\hat{\alpha})$;
2. Angle between the pen and the lower finger $(\hat{\alpha}')$;
3. Rate of change of the angle between the pen and the upper finger $(\dot{\hat{\alpha}})$;
4. Rate of change of the angle between the pen and the lower finger $(\dot{\hat{\alpha}}')$;
5. Tangential force felt by the upper finger $(\hat{F}_t)$;
6. Normal force felt by the upper finger $(\hat{F}_n)$;

7. Tangential force felt by the lower finger $\left(\hat{F}_t'\right)$;
8. Normal force felt by the upper finger $\left(\hat{F}_n'\right)$;
9. Upper finger's position $(\hat{r})$;
10. Lower finger's position $(\hat{r}')$;
11. Wrist's angle $\left(\hat{\theta}\right)$;
12. Upper finger's velocity $\left(\dot{\hat{r}}\right)$;
13. Lower finger's velocity $\left(\dot{\hat{r}}'\right)$;
14. Wrist's angular velocity $\left(\dot{\hat{\theta}}\right)$.

These variables are then manipulated in order to build a controller capable of performing the task of wiggling the pen in between the fingertips, in the sections to come.

4 Estimation of the pen's position

In order to detect the pen's position, the estimator is assumed to know the dimensions, the mass and the inertia of the pen and finger. Moreover, for detection to take place, a normal force must be detected on the fingers, marking the pen's presence known. If no forces are detected in either finger, then the pen is not detected, resulting in its position being assumed to be where it was last detected at.

4.1 Angle estimation

Firstly, from the manipulation of equation (2.14), the estimated angle of the pen $\hat{q}$ is calculated simply as the estimated angle of the wrist $(\hat{\theta})$ plus the estimated angle of contact $(\hat{\alpha})$,

$$\hat{q} = \hat{\theta} + \hat{\alpha}. \tag{4.1}$$

As the angle $\hat{\alpha}$ is only detected when there is contact with the pen, equation (4.1) is only valid when one of the fingers is in contact with the pen. By differentiating equation (4.1), the estimated pen's angular velocity is obtained as the sum of the angular velocity of the wrist and the contact's,

$$\dot{\hat{q}} = \dot{\hat{\theta}} + \dot{\hat{\alpha}}. \tag{4.2}$$

Due to the limitations of the sensory system, the angular acceleration of the wrist and the contact's is unknown and as such needs to be approximated. To do so, consider that there is a frequency at which the estimation of $\hat{\theta}$ and $\hat{\alpha}$ are precepted, in the muscle, [21, 22], and on the Merkel cells, Table 4, respectively. This frequency results in a time sample of 0.01 seconds, which can be used to estimate the angular acceleration, by subtracting the estimated angular velocity of the pen and the angular velocity estimated at a previous timestep and then dividing over the time sample, resulting in

$$\ddot{\hat{q}} = \frac{\dot{\hat{q}}_t - \dot{\hat{q}}_{t-1}}{T_s}. \tag{4.3}$$

4.2 Position estimation

Secondly, the position of the pen in relation to the fingers is estimated. To this end, the distance between the fingers is first calculated by using the angle at which the pen is felt on the finger $(\hat{\alpha})$ as follows.

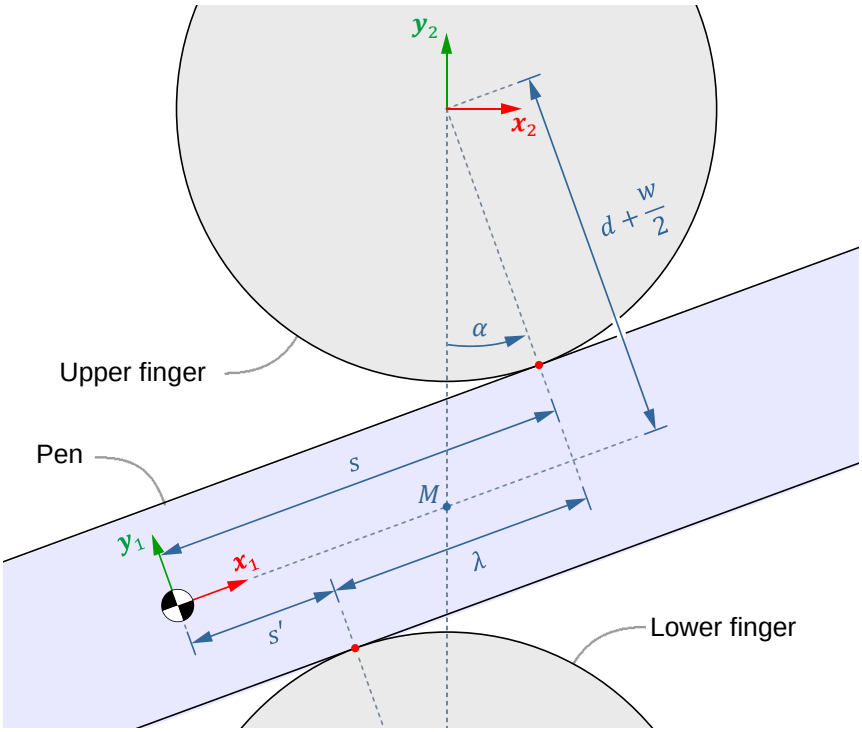

Figure 4.1 – Illustration of the pen between the fingers and definition of relevant variables for detection. The distance between the fingers, in the tangential direction of the pen, is given by λ. The x component of the distance from the pen's contact points to its center of mass, s and s' are defined. M is the intersection point between a line that joins the two fingers and the pen's x-axis, x_1.

As illustrated in Figure 4.1, the interfinger distance (λ) is estimated as

$$\lambda = 2\left(d + \frac{w}{2}\right)\tan(\hat{\alpha}). \tag{4.4}$$

Then, the forces felt on the fingers are used to estimate the forces affecting the pen, on the upper contact point

$$\widehat{\boldsymbol{F}}_1 = \widehat{\boldsymbol{R}}_2^1\left(-\widehat{\boldsymbol{F}}_2\right), \tag{4.5}$$

and lower contact point

$$\widehat{\boldsymbol{F}}_1' = \widehat{\boldsymbol{R}}_{2'}^1\left(-\widehat{\boldsymbol{F}}_2'\right). \tag{4.6}$$

These forces are used to estimate the distance they span from the center of mass of the pen by equating all the torques applied on the pen and its apparent rotation on the fingers. Towards this end, the distances from the upper finger and the lower finger to the center of mass of the pen, s and s', are first related to the interfinger distance, as

$$\hat{s} = \lambda + \hat{s}'. \tag{4.7}$$

Also, the position vectors for both contact points ($\hat{\boldsymbol{c}}_1$ and $\hat{\boldsymbol{c}}_1{}'$) on the pen are able to be estimated as

$$\hat{\boldsymbol{c}}_1 = \begin{bmatrix} \hat{s} & \frac{w}{2} & 0 \end{bmatrix}^T \tag{4.8}$$

and

$$\hat{\boldsymbol{c}}_1' = \begin{bmatrix} \hat{s}' & -\frac{w}{2} & 0 \end{bmatrix}^T. \tag{4.9}$$

Then the torque balance can be equated, resulting in

$$I_{z,p}\, \ddot{\hat{q}} = \hat{\boldsymbol{c}}_1 \times \hat{\boldsymbol{F}}_1 + \hat{\boldsymbol{c}}_1' \times \hat{\boldsymbol{F}}_1'. \tag{4.10}$$

where $I_{z,p}$ is the inertia of the pen. Now, introduction of equations (4.7), (4.8) and (4.9) into (4.10), results in

$$I_{z,p}\, \ddot{\hat{q}} = -\hat{F}_t\, \frac{w}{2} + \hat{F}_n\, \hat{s} - \hat{F}_t' \left(-\frac{w}{2}\right) + \hat{F}_n'\, \hat{s}' \tag{4.11}$$

and the distance from the fingers to the center of mass can be solved as

$$\begin{cases} \hat{s}' = \dfrac{I_{z,p}\ddot{\hat{q}} + \frac{w}{2}\hat{F}_t - \lambda\, \hat{F}_n - \frac{w}{2}\hat{F}_t'}{\hat{F}_n - \hat{F}_n'}, \\ \hat{s} = \lambda + \hat{s}'. \end{cases} \tag{4.12}$$

With the distances between the center of mass and each finger calculated, the distance between the mass center and point M can now be calculated as the average of both distances, in the opposite direction. Thus, the displacement from point M towards the mass center can be estimated, in the world frame, as

$$\hat{\boldsymbol{r}}_{M,1} = \hat{\boldsymbol{R}}_1^0 \begin{bmatrix} -\left(\frac{\hat{s}+\hat{s}'}{2}\right) \\ 0 \\ 0 \end{bmatrix}. \tag{4.13}$$

The next step is to calculate the contribution of the fingers' position to the position of the pen's center of mass. Towards this end, a line is imagined connecting the fingers vertically, like done in Figure 4.2.

Then the vertical distance from the point M to the axis z_0, Υ, is estimated, illustrated in Figure 4.2. In the simple case where both fingers are in contact with the pen, this height comes up to the average of the fingers' estimated distance to the wrist $\hat{r}$ and $\hat{r}'$, given as

$$\Upsilon = \frac{\hat{r} - \hat{r}'}{2}, \qquad \text{adjacent to both fingers.} \tag{4.14}$$

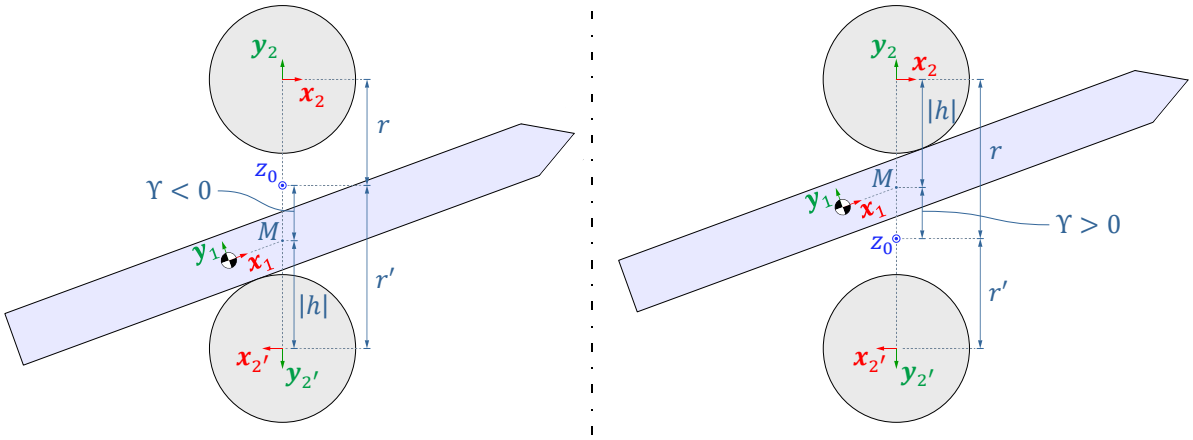

Figure 4.2 – More relevant variables for detection. A vertical dotted line connects the two fingers. The intersection between this line and the pen's x_1 axis is the point M, marked by a blue circle. $|\Upsilon|$ is the distance between the z_0 axis and point M and it is measured positively along y_2. The distance between M and the finger in contact with the pen is denoted as h. On the left the pen is adjacent to the lower finger, while on the right it is adjacent to the upper finger.

However, if the pen is only in contact with one of the fingers, as seen on Figure 4.2, Υ can be calculated as the distance h from the finger, calculated according to the Pythagoras' theorem as $(\delta \approx 0)$

$$h = \sqrt{\left(\frac{\lambda}{2}\right)^2 + \left(d + \frac{w}{2}\right)^2} \tag{4.15}$$

and the finger's distance to the wrist, $\hat{r}$,

$$\Upsilon = \begin{cases} \hat{r} - h, & \text{adjacent to upper finger,} \\ h - \hat{r}', & \text{adjacent to lower finger.} \end{cases} \tag{4.16}$$

Finally, the center of mass from the contribution of the fingers' position can be calculated as

$$\hat{\boldsymbol{r}}_{0,M} = \hat{\boldsymbol{R}}_2^0 \begin{bmatrix} 0 \\ \Upsilon \\ 0 \end{bmatrix} \tag{4.17}$$

The position of the center of mass of the pen is then the sum of both contributions in equations (4.13) and (4.17)

$$\hat{\boldsymbol{p}}_1 = \hat{\boldsymbol{r}}_{0,M} + \hat{\boldsymbol{r}}_{M,1}. \tag{4.18}$$

4.3 Validation

Firstly, to validate the solution described in the aforementioned sections, the real pen's angular acceleration was used instead of the estimated one in equation (4.3) in order to estimate the pen's position through a simple exercise, where the fingers remain immobile and 16 centimeters apart (more than the pen's width). Also, the pen is initialized with its center of mass at the coordinates $(x, y, z) =$

$(2, 0, 0)$ centimeters and with an initial angle of 0 (horizontal). This exercise leads to the pen falling onto the lower finger and slipping to the side it is offset to, leading to contact with the upper finger as it rotates around the bottom one. As this happens, the friction from the slippage on both fingers brings the pen to a stop. For this exercise, the estimated position and position error of the pen, in relation to time, are plotted in Figure 4.3. The estimated angle of the pen does not depend on the estimated angular acceleration and thus is perfectly accurate. As such, it is not plotted.

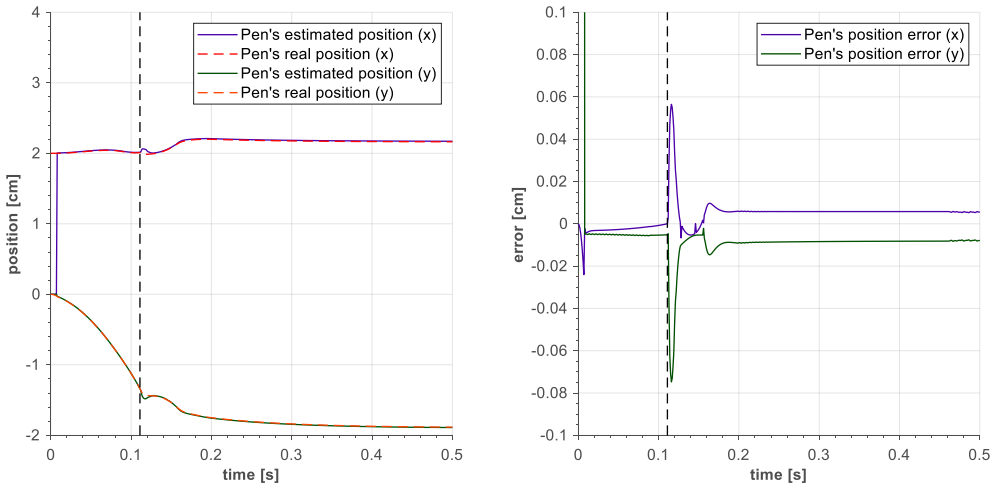

Figure 4.3 – Validation of the estimation of the position of the pen using its exact angular acceleration. On the left, the x and y components of the pen's estimated position and real position. On the right, the pen's position error. In black, a vertical line illustrates the time at which contact takes place.

As seen in Figure 4.3, the pen's position is well estimated by the solution, so much so that the graph lines for the real position of the pen are barely visible due to them being obstructed by the estimation data, except for the first instant when the system is initialized. Thus, it is concluded that the validation is successful and the solution is working as intended.

Secondly, the angular acceleration estimated in equation (4.3) is compared to the true angular acceleration of the pen so as to assess the accuracy of the estimation being made. Given the exercise, meaningful angular accelerations are observed at the moment of contact, marked by a black vertical line in Figure 4.4, at around 0.11 seconds.

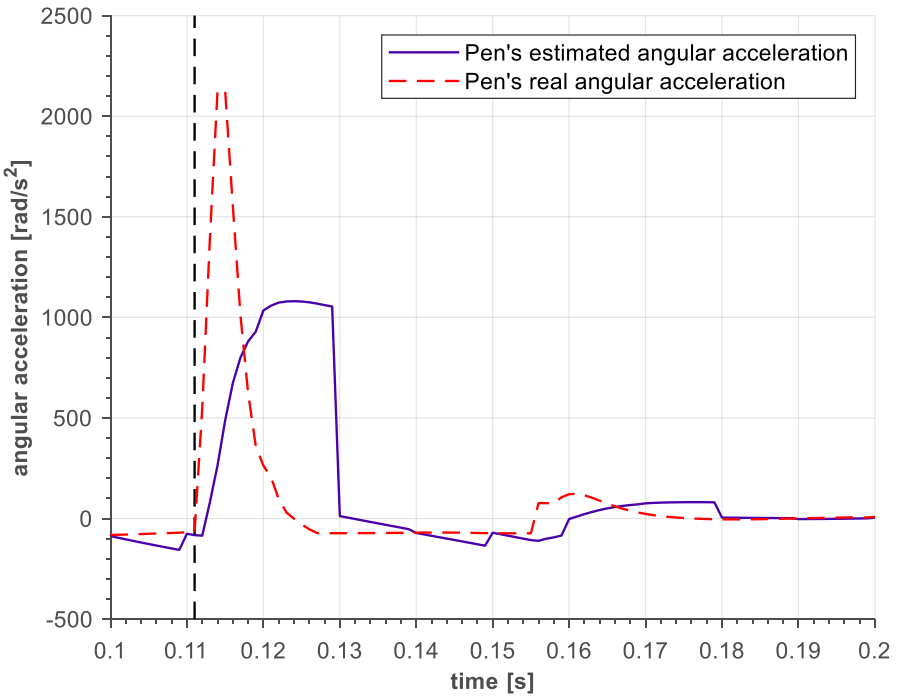

Figure 4.4 – Estimation of the pen's angular acceleration and its real angular acceleration, compared. In black, a vertical line illustrates when contact takes place.

Analyzing Figure 4.4, it is clear that the estimated pen's angular acceleration roughly follows its true angular acceleration. When the true angular acceleration has very high values though, or when these values have a high rate of change, the estimated angular acceleration does not match the true values well. The impact of this mismatch on the prediction of the pen's position is heavy, illustrated in the next figure.

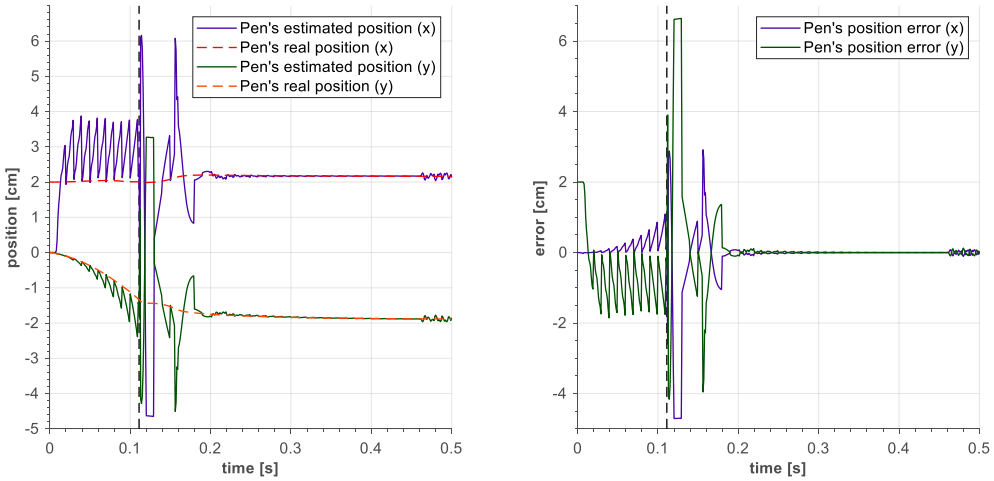

Figure 4.5 – Estimation of the position of the pen using its estimated angular acceleration. On the left, the x and y components of the pen's estimated position and real position. On the right, the pen's position error. In black, a vertical line illustrates when contact takes place.

Right away, signal spikes can be seen in Figure 4.5. This is due to the time sample ($T_s = 0.01\ s$) used in the calculation of the estimated angular acceleration, which resets the values for the estimated position to reasonable ones at that rate. Due to this roughness, the estimation of the pen's position is rough as well when fast movements are concerned. In the first 0.1 seconds, there is some smooth movement of the pen (rolling on the lower finger) and, as such, the estimation of the pen's position is somewhat accurate for its y component and rough for its x component. At around 0.11 seconds the pen suffers an abrupt stop as it collides with the upper finger and therefore suffers high angular accelerations (visible in Figure 4.4 as the angular acceleration spikes). Given the accuracy lost in the estimated angular acceleration, the estimated position also loses some accuracy and deviates from the real position. After the collision, the estimator is accurate as the angular acceleration is smooth throughout the rest of the event.

Regarding the estimated angle of the pen, it can be estimated smoothly throughout the whole event, as it is not computed from the estimated angular acceleration.

5 Controller

The purpose of the controller is to make the pen oscillate from side to side, in between the fingers. The goal is for this oscillation to be a smooth movement. For this to be feasible, the grasping force on the pen cannot either be too much, as it would restrict the pen's movement, nor too little, as it would lead to the pen slipping off its grasp.

In this section a controller is introduced that is composed of three parts. These parts consist of a controller for the finger's position, an impedance controller for stable grasping and an object manipulation controller. The first two controllers produce a control action of force that, summed, represent the control action of force, applied on the finger joints. The third controller produces an action of torque, applied to the wrist.

5.1 Finger position control

The control of the position of the fingers is essentially needed to keep the fingers close and equidistant to the wrist's axis of rotation, as well as to dissipate energy associated with the movement of the fingers. Towards this end, the center-point of the fingers, $(r - r')/2$, is controlled as a critically damped system and the radial velocity of the fingers, $\dot{r}$ and $\dot{r}'$, is fed back negatively. Thus, the control action for the upper finger is given as

$$F_1 = K_{p,f}\left(r_r - \frac{(r - r')}{2}\right) + K_{d,f}\left(\dot{r}_r - \frac{(\dot{r} - \dot{r}')}{2}\right) - K_{v,f}\,\dot{r} \tag{5.1}$$

where r_r and $\dot{r}_r$ are the reference position and the reference velocity for the center-point of the fingers, respectively, which are set to zero as it is intended that the finger's center-point be positioned on the wrist's axis of rotation. K_p, K_d and K_v are the control gains regarding the position and velocity of the center-point of the fingers and velocity of the fingers, respectively. Similarly, the equivalent symmetric control action is used for the lower finger, with its respective velocity, $\dot{r'}$

$$F_1' = K_{p,f}\left(r_r - \frac{(r - r')}{2}\right) + K_{d,f}\left(\dot{r}_r - \frac{(\dot{r} - \dot{r}')}{2}\right) - K_{v,f}\,\dot{r}'. \tag{5.2}$$

Consider the displacement of the center point due to gravity alone. Then, for an allowable deviation from the wrist's axis of rotation of about 0.5 millimeters, K_p can be calculated such that

$$K_{p,f}(5 \times 10^{-4}) = \left(m_p + 2m_f\right)g, \tag{5.3}$$

where m_p is the pen's mass, m_f is the mass of one finger and g is the acceleration of gravity. Assuming that the system is linear, this results in a control gain of $K_{p,f} \approx 729$, from which follows for a critical damping $K_{d,f} = 2(m_p + 2m_f)\sqrt{\frac{K_{p,f}}{m_p+2m_f}} = 10.4$. Lastly $K_{v,f}$ was determined experimentally, resulting in $K_{v,f} = 10$.

5.2 Stable grasping impedance

For stable grasping, there needs to be a grasping force such that the frictional force between the pen and the fingers is enough to not let the pen slip but not too much that it overly restricts the pen's movement. The control action employed for this task, for the upper finger, consists in a proportional control where a reference penetrating distance on the pen is set [10], given as

$$F_2 = -K_{p,\delta}(\delta_r - \hat{\delta}), \tag{5.4}$$

where δ_r is a reference value for the penetrating distance and $K_{p,\delta}$ is a control gain. The current estimated penetrating distance, $\hat{\delta}$, is calculated according to equation (2.6), where the pen's position is estimated, $\hat{\boldsymbol{p}}_1$, through equation (4.18). Equivalent control action is used for the lower finger.

$$F_2' = -K_{p,\delta}(\delta_r - \hat{\delta}'), \tag{5.5}$$

Figure 5.1 compares both $\hat{\delta}$ and δ, on the two fingers. To note that the upper finger detection is much more reliable than the lower one's. As the upper finger is more important for the control of the system, which allows the pen to rotate, than the lower one which holds the pen, this discrepancy in reliability of the penetration distance is not disruptive.

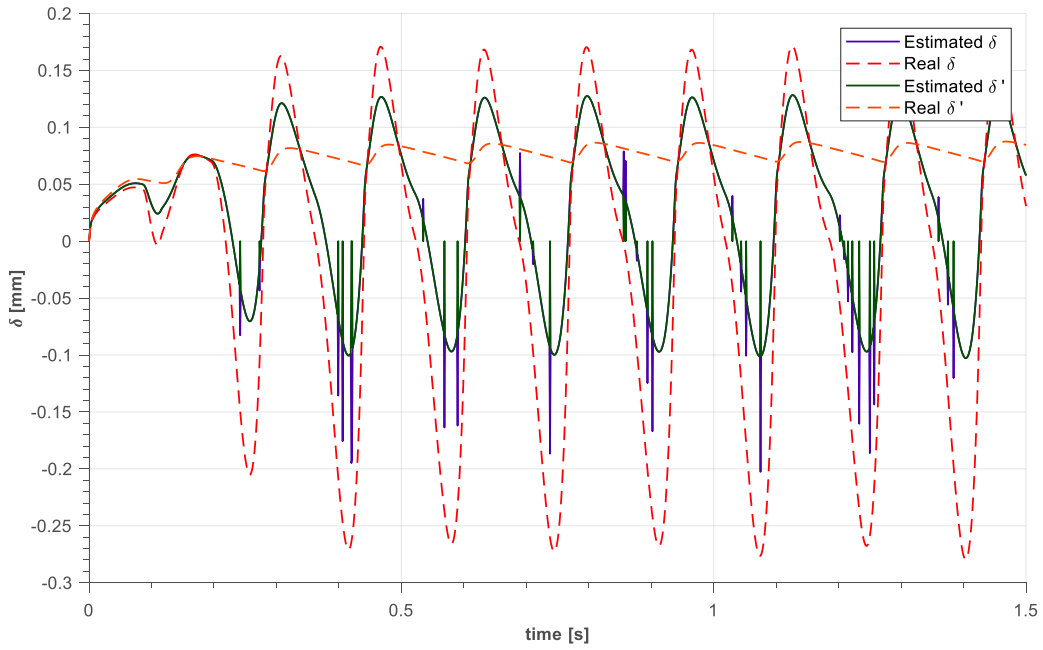

Figure 5.1 – Estimation of the penetration distance $\hat{\delta}$ and real penetration distance δ, for both fingers. The input reference signal is a sine wave of amplitude of $A = 0.7$ and frequency $\omega = 19\, rad/s$.

Consider now an exercise where the pen is held vertically between the fingers, such that the only force counter acting the pen's weight is the frictional force, resulting in

$$F_t = m_p g, \tag{5.6}$$

where m_p is the pen's mass and g is the gravity constant. Splitting the frictional force, so that each finger is applying half of this force on the pen and considering the state of dynamic friction between the bodies (as it is the least stable state), then the normal force to be applied on the pen by each finger is

$$F_n = \frac{m_p g}{2\mu_d}. \tag{5.7}$$

Now, the penetration distance equivalent to such normal force, δ^*, can be obtained from equation (2.19), in stationarity $\dot{\delta} = 0$, therefore $K(\dot{\delta}) = k$, yielding

$$\delta^* = \sqrt[a]{\frac{1}{k}\frac{mg}{2\mu_d}}, \tag{5.8}$$

resulting in $\delta^* \approx 5.2 \times 10^{-5}$.

Then, by choosing suitable values for the reference of the penetrating distance δ_r and the control gain $K_{p,\delta}$, an optimum grasping force can be reached. That said, setting $\delta_r = 8 \times 10^{-5}$, $K_{p,\delta}$ can be calculated from

$$\frac{mg}{2\mu_d} = K_{p,\delta}(\delta_r - \delta^*), \tag{5.9}$$

resulting in $K_{p,\delta} \approx 2.63 \times 10^3$.

5.3 Object manipulation impedance

The manipulation of the object, adapted from [10], is intended towards the object's angle. In such case, the dynamics of the object are governed by

$$T + T_{ext} = I_{z,p}\ddot{q} \tag{5.10}$$

where T is the manipulation torque exerted on the object by the fingertips, T_{ext} is an external perturbation torque and $I_{z,p}$ is the actual inertia of the pen. The desired interaction of the system is given as

$$T_{ext} = I_{z,d}\ddot{q} + D_T(\dot{q} - \dot{q}_r) + K_T(q - q_r) \tag{5.11}$$

where q_r and $\dot{q}_r$ are the reference angular trajectory, $I_{z,d}$ is the desired apparent inertia and D_T, K_T are the damping and stiffness, respectively. As described in [10], by keeping the inertia unchanged, $I_{z,d} = I_{z,p}$. Then, since $T_{ext} = I_{z,p}\,\ddot{q} - T$, the impedance control law is

$$T = K_T(q_r - \hat{q}) + D_T(\dot{q}_r - \dot{\hat{q}}) \tag{5.12}$$

The control gains were manually tuned, set at $K_T = 10$ and $D_T = 0$, as the presence of overshoot in the angle of the pen is actually beneficial for this task (oscillation of the pen) and therefore no damping is required.

5.4 Block diagram

The block diagram for the control method employed, discussed in the above sections, is illustrated in Figure 5.2.

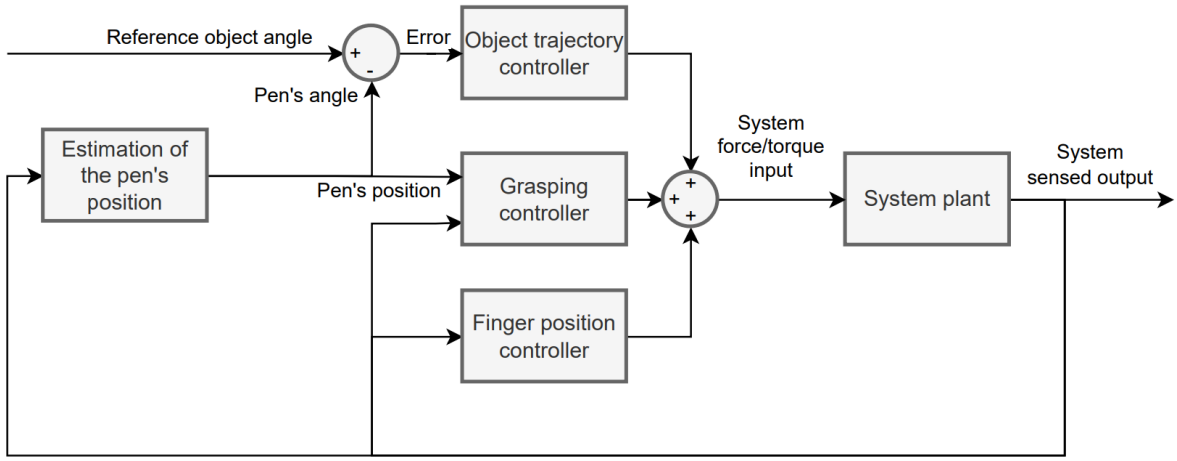

Figure 5.2 – Block diagram for the control methods employed, detailed throughout sections 4 and 5.

5.5 Analysis and discussion

The control action can then be summed up as a force of grasp for the upper and lower fingers, $F = F_1 + F_2$ and $F' = F_1' + F_2'$, respectively, and a torque for the wrist, T. The system was then given a reference signal for the pen's angle, q, corresponding to a sine wave of amplitude $A = 0.7$ and frequency $\omega = 19\, rad/s$. The pen's starting position was the origin with mass center along z_0. The controlled action was recorded and is displayed in Figure 5.3, below. To note that the positive direction of torque about z_0 is the anti-clockwise rotation direction and regarding the force of the fingers, a positive force along y_2 and y_2' results in the opening of the upper finger and lower finger, respectively, and a negative force results in the closing of the finger.

On Figure 5.3, the input torque is, expectedly, very similar to the reference signal, cyclical with matching frequency, as the wrist performs the torque needed required for the torque applied on the pen to match the reference trajectory.

Regarding the fingers, it is noticeable that the lower finger produces more closing force than the upper finger, due to the need of having to hold the pen's mass and acting as a support rather than shaping the pen's movement. The upper finger however has both positive and negative forces, meaning that it both performs an opening and closing force on the pen. This is expected for the task at hand, as it requires the upper finger, to at times, open and allow for the pen to roll, while at other times it is expected to close and produce a rotating motion in the other direction, thus oscillating the pen on the fingertips. It is noticeable that this movement of the fingers is cyclical and has double the frequency of the reference signal.

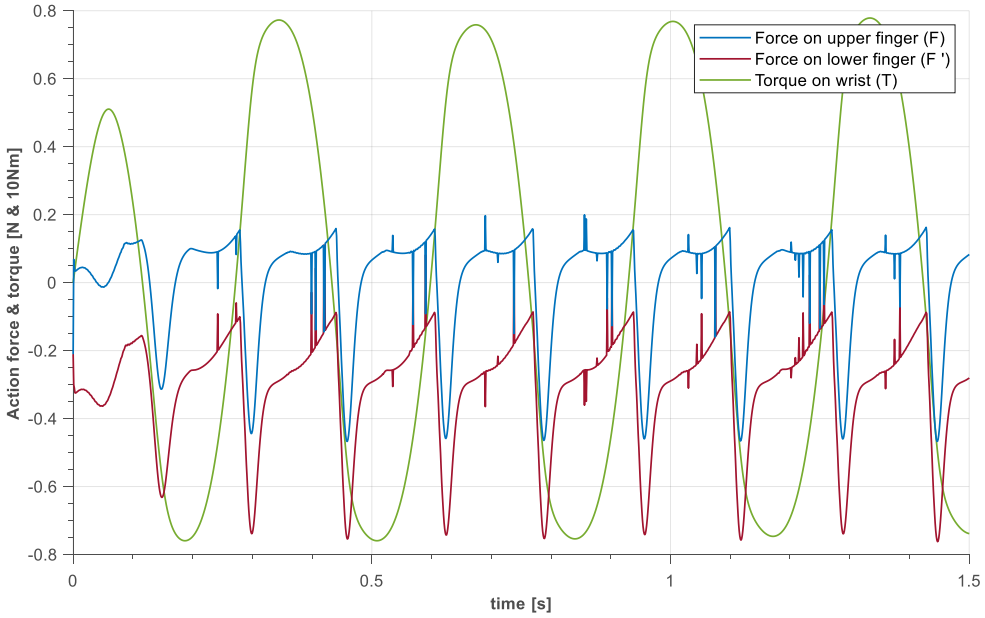

Figure 5.3 – Controller action to follow the reference of a sine wave of amplitude of $A = 0.7$ and frequency $\omega = 19\ rad/s$. The positive direction of torque is anti-clockwise and a positive force on the fingers equates to the opening of the finger, while the negative force equates to the closing of the finger.

The system was run for a longer duration, with similar cyclical behavior. The controller proved to be robust against the slippage of the pen and effective, oscillating the pen according to the reference given. In Figure 5.4, the reference is compared to the pen's trajectory.

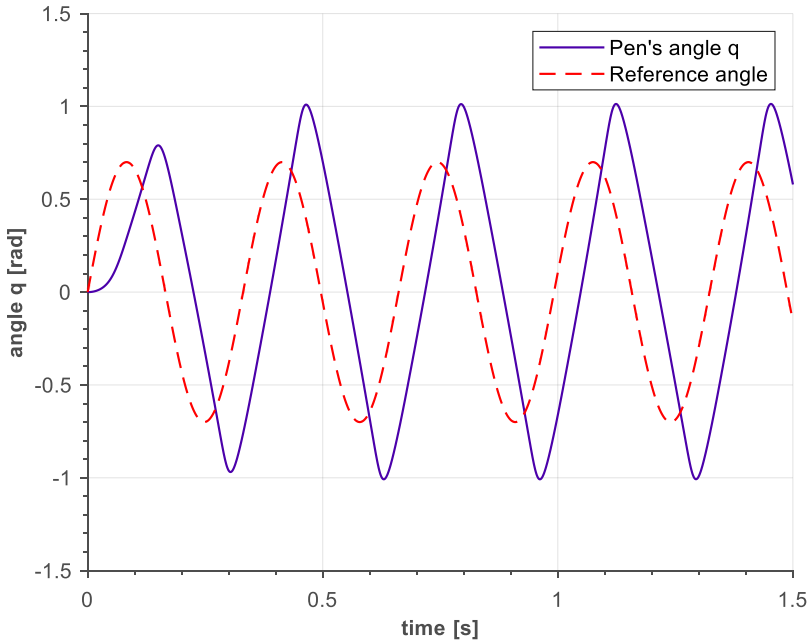

Figure 5.4 – Reference signal for the pen's angle and the pen's angle q, side by side. The reference signal is a sine wave with amplitude $A = 0.7$ and frequency $\omega = 19\ rad/s$.

As illustrated in Figure 5.4, the pen's angle, q, roughly follows the reference signal provided, q_r. Due to the construction of the controller, some overshoot exists, which is beneficial as it reflects in a larger oscillation on the pen. It is noticeable that there is some tracking error in the system, which is not meaningful as for this task it is not essential. The controller is deemed successful as it performs the task of oscillating the pen while maintaining a grasp on it, with the reference conditions.

5.6 Analysis and discussion of the pen's estimated position, governed by the controller

Now the accuracy of the observer is assessed in the proposed use case, see section 1.2, where the pen is oscillated in between the fingertips, governed by the controlled. The pen was initialized with its center of mass between the fingertips (at the origin) and an input of a desired pen angle was given, as a sine wave with frequency $\omega = 19\,rad/s$ and amplitude $A = 0.7$. This frequency was experimentally determined as being the resonant frequency of the closed-loop system (see section 6.2) [23]. The prediction of the pen's position, $\hat{\boldsymbol{p}}_1 = (\hat{x}, \hat{y}, 0)$ is shown below, as well as the true pen's position $\boldsymbol{p}_1 = (x, y, 0)$. The prediction of the angle $\hat{q}$ is not affected by the inaccuracy of the estimated angular acceleration as mentioned above and as such will not be discussed.

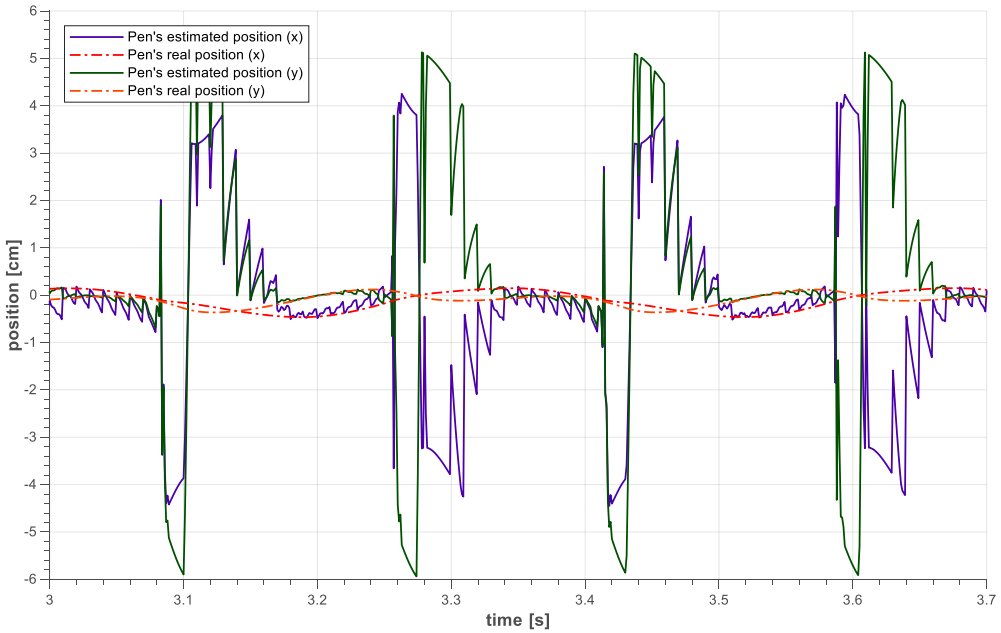

Figure 5.5 – Plot of the estimated and real position of the pen, side by side. The time window is that of two system cycles, that is, $4\pi/\omega$. The input reference signal is a sine wave of amplitude of $A = 0.7$ and frequency $\omega = 19\,rad/s$.

In Figure 5.5, the signal spikes due to the time sample used for the angular acceleration are seen again. It is evident that the mismatch of the angular acceleration for quick movements results in a mismatch in the prediction of the pen's position in the systems intended use case, which is the fast

oscillation of the pen on the fingertips. The mismatched spikes are observed at the instants where the pen is under high angular accelerations, when the fingertips force it to oscillate in the other direction (time window of 3.08 to 3.16 seconds). At these moments, the prediction has an error of about 5 cm in both the x and y components of the pen's position, a significant error considering that the pen's width and length are 8 mm and 13.2 cm respectively.

When the pen is not under such angular accelerations, at moments when it is rolling on the finger, the detection of the pen's position is reliable (time window of 3.16 to 3.24 seconds), having a small amount of error in both components of the pen's position.

All in all, half of the time, the detection of the pen's position is reliable. This will prove to be enough for the controller, as discussed in this section.

6 System's response analysis and exploration

For the analysis of the system's response, it is important to define the trajectory of the pen and the phases of the rotation cycle. In Figure 6.1, these phases are depicted.

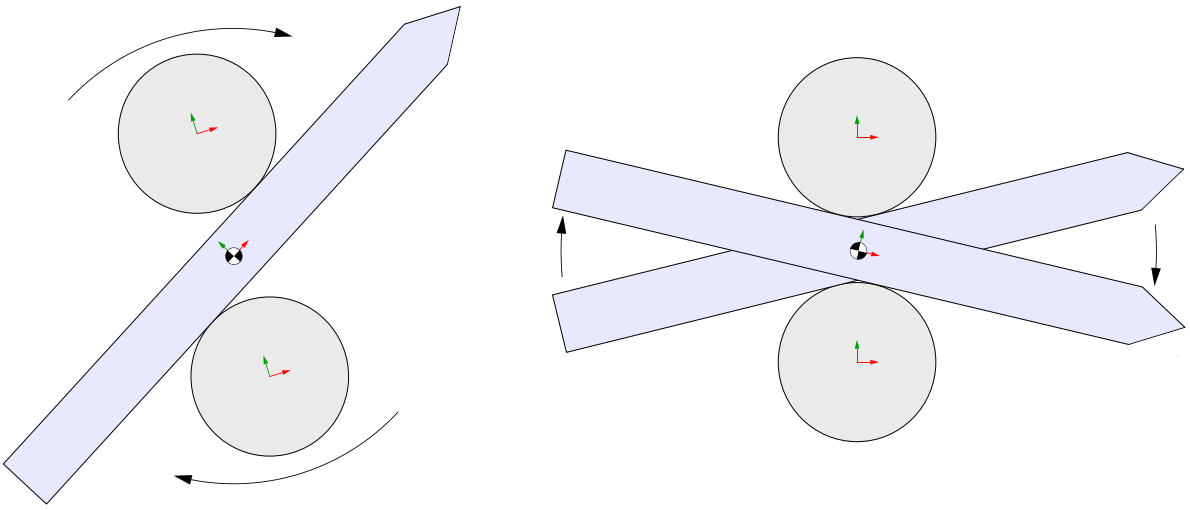

Figure 6.1 – Representation of a half-cycle of the pen oscillation movement on the fingers. On the left, negative twisting, on the right, negative rolling. The next half-cycle of the movement would consist of these same two movements, in the positive direction of rotation.

The phases in a cycle are four: negative twisting, negative rolling, positive twisting, and positive rolling. This movement is similar in each half-cycle, where the only difference is the direction of the movement. In the twisting phase the fingers apply a torque on the pen which forces is to change the direction of its rotation and begin to spin. In the rolling phase, the fingers apply a small amount of torque and let the pen spin freely.

The system can now be explored in terms of robustness to the pen's slippage and response. It was made to follow the reference of the pen's angle, q_r. The reference signal of q_r is a sine wave with amplitude A and frequency ω. Below, an analysis of a simplified linearized system is discussed. Further below, an analysis of the system's response is discussed, along with its robustness to slippage and a comparison to the simplified linearized system.

In Figure 6.2, a sequence of frames that illustrate the action of oscillating the pen on the fingertips is drawn. The frames were sampled at 40 Hz and enough frames are illustrated to show one cycle of the system at its resonant frequency, which will be introduced in section 6.1, of $\omega = 19\,rad/s$. The phases described in Figure 6.1 can be seen. In Figure 6.3, a sequence of frames at a higher frequency is shown ($\omega = 58\,rad/s$).

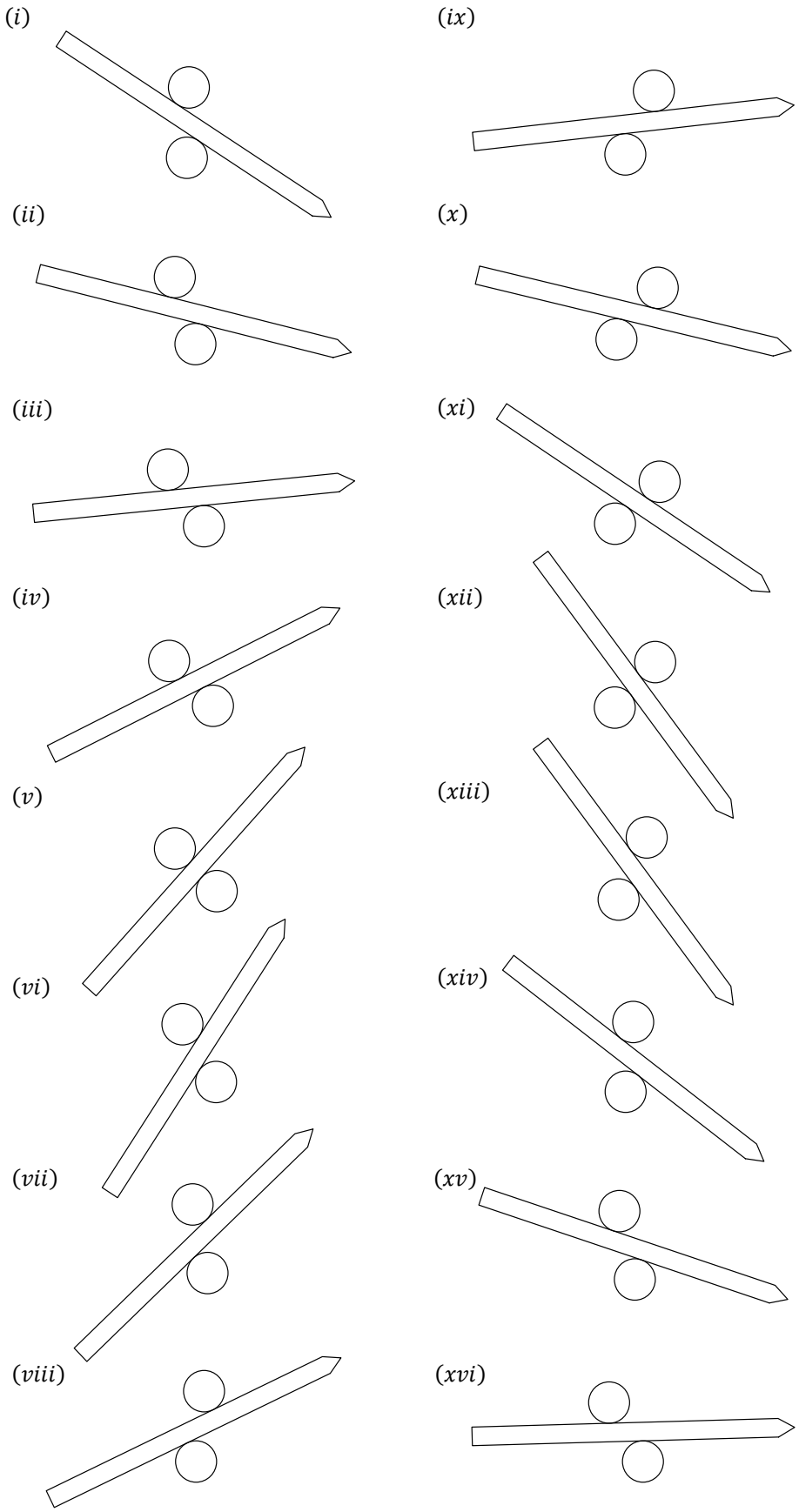

Figure 6.2 – Sequence of frames of the action of oscillating the pen on the fingertips. The reference signal has a frequency of 19 rad/s and one cycle is illustrated. Sampled from simulation at 40 Hz.

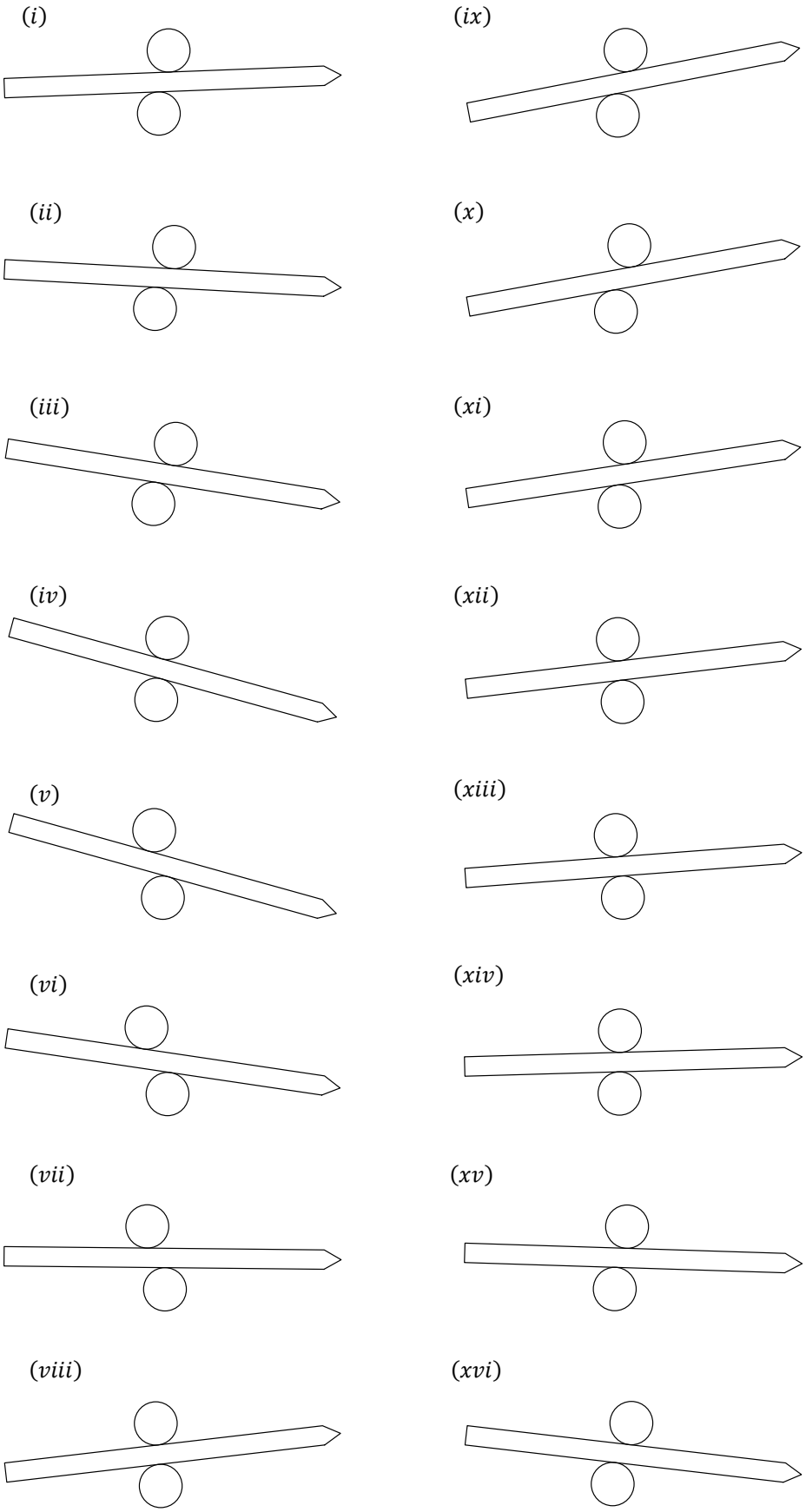

Figure 6.3 – Sequence of frames of the action of oscillating the pen on the fingertips. The reference signal has a frequency of 58 rad/s and two cycles are illustrated. Sampled from simulation at 62.5 Hz.

6.1 Linearized system analysis

Before analyzing the model, a simplification of the system was performed with the intent of calculating the system's resonant frequency, which could be compared with the model's, through its linearization. This simplified system is depicted in the next figure, a recall from Figure 2.5 and Figure 2.6.

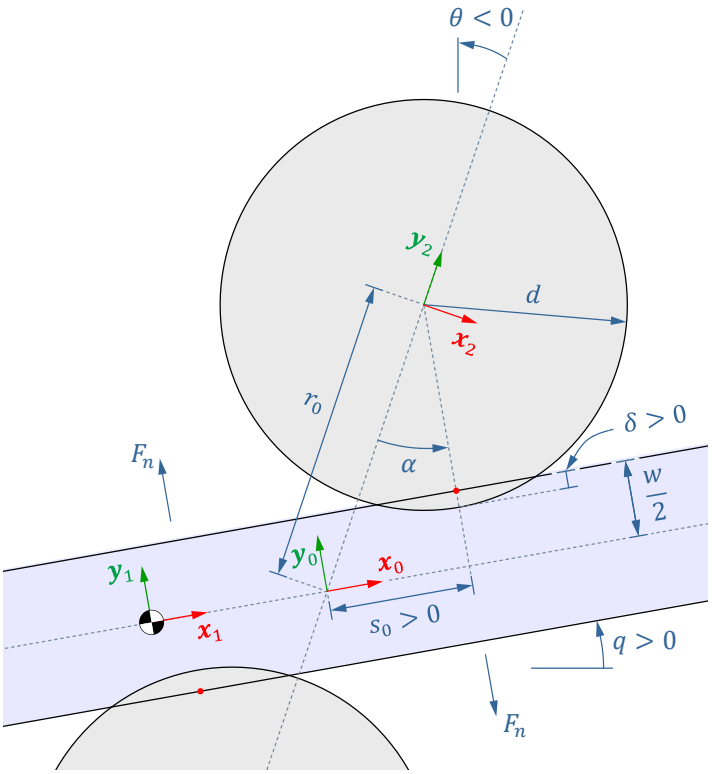

Figure 6.4 – Representation of important variables for the simplified system.

The system was considered to have an imposed trajectory on the wrist's rotation, θ, as a harmonic oscillator in the form of $\theta(t) = B\,\sin(\omega t + \phi_0)$. The dynamics between the pen and the fingers can be equated as

$$I_{z,p}\ddot{q} = -2\,s_0\,F_n, \tag{6.1}$$

where F_n is the normal force, as stated in (2.19), in the simplified form of

$$F_n = Ke^{\eta\dot{\delta}}\delta^a. \tag{6.2}$$

From Figure 6.4, with some manipulation, the system can be written as only a function of α, as $s_0 = \mathrm{r}_0\,\sin(\alpha)$ and $\delta = (d + w/2 - r_0\cos(\alpha))$, thus becoming

$$I_{z,p}\ddot{q} = -2\,K\,r_0\sin(\alpha)\,e^{\eta\,r_0\,\sin(\alpha)\dot{\alpha}}\left(d + \frac{w}{2} - r_0\cos(\alpha)\right)^a, \tag{6.3}$$

By linearizing the system around $\alpha = 0$, the first term of Taylor series will be

$$\tilde{\tau} = \frac{\partial \tau}{\partial \alpha}\Big|_{\alpha=0} \alpha = -2\,K\,r_0\left(d + \frac{w}{2} - r_0\right)^a \alpha \tag{6.4}$$

with $\alpha = q - \theta$. Bearing in mind $\ddot{q} = -\omega_r^2\, q$ is the solution to a harmonic oscillator, and $\theta = 0$ in this linearization, then $q = \alpha$ and

$$\ddot{q} = -\omega_r^2\, \alpha \tag{6.5}$$

from which results, by substitution in (6.4),

$$\omega_r = \sqrt{\frac{2\,K\,r_0\left(d + \frac{w}{2} - r_0\right)^a}{I_{z,p}}} = \sqrt{\frac{2\,K\,\left(d + \frac{w}{2} - \delta\right)\delta^a}{I_{z,p}}}. \tag{6.6}$$

The resonant frequency, ω_r, can then be calculated by using mean values for the penetration distance δ. It varies with the frequency, with values between $6 \times 10^{-5}\, m$ to $8 \times 10^{-5}\, m$ (δ and δ' from the analysis Figure 5.1. Extra weight was given to δ' as due to the dynamics of the system, δ has large variations in its value as the upper finger moves up and down, as the system starts its rolling phase). This results in a resonant frequency for the system of $18.3\, rad/s$ to $22.7\, rad/s$.

6.2 Response of the system to frequency

The system was evaluated through a range of frequencies, from 1 to 60 rad/s and an amplitude of 0.7. Its response was analyzed and the pen's maximum angle q_{max} as well as the hand's maximum angle θ_{max}, in absolute value, were recorded. Figure 6.5 illustrates the systems response to such frequencies.

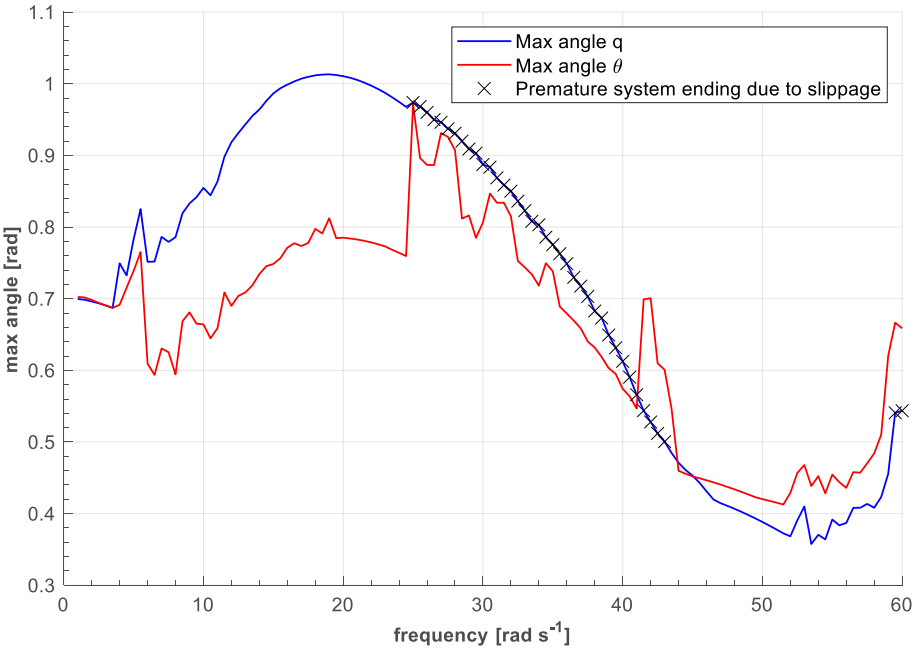

Figure 6.5 – Response of the system to a reference input on the pen's angle of a sine wave of amplitude $A = 0.7$ and frequency of ω, ranging from 1 to 60 rad/s, simulated for 5 seconds. The pen's absolute value of maximum angle, q_{max}, is drawn in blue, while the wrist's absolute value of its maximum angle, θ_{max}, is drawn in red. Black crosses are also illustrated, representing frequencies at which the system ended prematurely due to the pen slipping off the fingertips' grasp.

From Figure 6.5, it is clear by inspection of the lower frequency responses that there is a minimum frequency at which the pen begins to oscillate, which is at around 4 rad/s. At frequencies below this, the maximum angle of both the pen and the wrist match, implying the pen is not allowed to oscillate and is simply being rotated by the fingers while grasped tightly.

At frequencies of 4 to 25 rad/s the pen begins to oscillate, as is possible to see in Figure 6.5, by the difference in value between both lines. This difference equates to the amount of oscillation on the pen, as the wrist need only rotate some angle θ for the pen to rotate a larger angle q. This happens due to there being some leeway on the pen's rotation during the rolling phase. The higher the frequency at which the system operates, the larger the max angle values for both the pen and the wrist are. The difference between these angles, corresponding to the magnitude of the oscillation $q - \theta$, steadily increases with the increase in frequency, achieving a maximum at around 19 rad/s, illustrated on Figure 6.2. The maximum values for q also reach a maximum at this frequency. This observation matches up with the resonant frequency calculated in the linearized system in section 6.1 and therefore, the system's resonant frequency is confirmed to be of around 19 rad/s. The system proves to be stable for this range of frequencies.

At frequencies larger than 25 rad/s, the system becomes unstable, depicted in Figure 6.5 by black crosses on the frequency level at which the system let the pen escape its grasp. This also resulted in the lowering of the magnitude of oscillation as the wrist tries to compensate for the slippage of the pen. It is also noticeable that starting at this frequency of 25 rad/s, the increase of the reference frequency leads the maximum angle of both the pen and the wrist to decrease in value. This is a result of the system operating at a higher frequency than its resonant oscillating frequency, thus not allowing the pen to fully complete its rolling phase before being acted upon by an opposing torque on the twisting phase, and also due to the system letting the pen slip before managing to oscillate it.

Curiously, at frequencies of about 45 rad/s, the system becomes stable once again, but the magnitude of the oscillation becomes negative as the maximum rotation of the wrist, θ_{max}, becomes larger than the maximum rotation of the pen, q_{max}. As previously mentioned, this indicates that the system is operating at a higher frequency than its resonant frequency, resulting in the pen barely being able to conduct its rolling phase as the twisting phase forces the pen to change its direction of rotation, forcing an abrupt stop on the rolling phase. This behavior is illustrated in Figure 6.3.

Finally, at around 60 rad/s, the system becomes once again unstable, with similar characteristics to the high frequencies in regard to its phases. High frequencies proved to be very computationally intensive to run in simulation and, as a result, frequencies larger than 60 rad/s were not analyzed.

6.3 Cyclical behavior analysis: low and resonant frequency

To analyze the periodicity of the system, at frequencies ranging from 4 to 20 rad/s and an amplitude of 0.7, the parametric plotting of some key variables, such as the pen's angle and angular velocity, q and $\dot{q}$, together with the wrist's angle, θ, is of great value. Given the periodic response of the system, the following parametric plots have a period equal to two cycles of the input forced reference frequency, $\Delta t = 4\pi/\omega$.

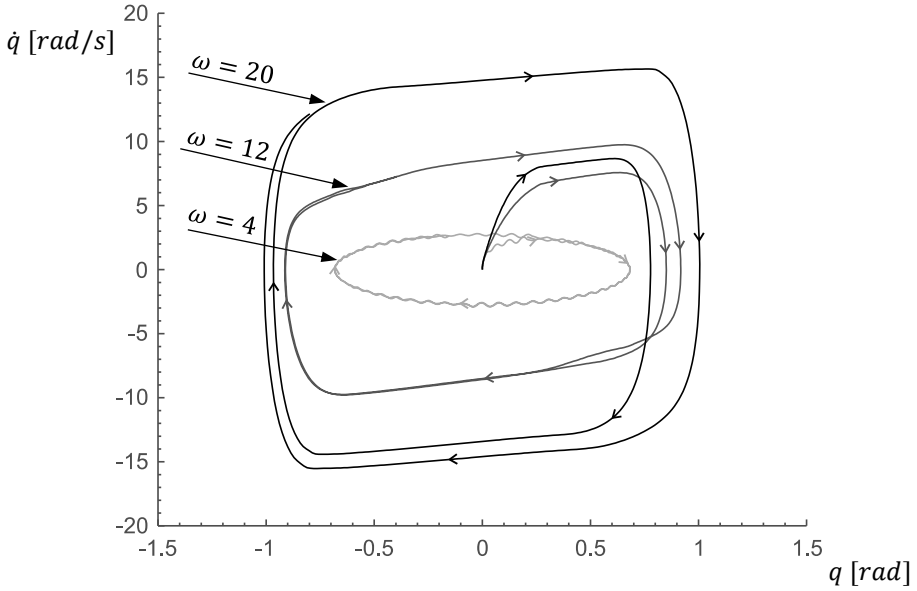

Figure 6.6 – Parametric plot of the pen's angle q and the pen's angular velocity $\dot{q}$. Three different system responses are plotted at three different input frequencies, 4, 12 and 20 rad/s. The responses were recorded over a time period of $4\pi/\omega$ of the input frequency.

From Figure 6.6, the parametric plot has a square shape through all three frequencies and the successive cycles reinforce the square shape, meaning cyclical behavior was reached [24]. The twisting phases and the rolling phases can be distinguished in this plot as they are represented by the vertical edges and horizontal edges of the shape, respectively.

The impact of the input frequency on the system is very noticeable. An increase in the input frequency equates to faster and more abrupt twisting and rolling phases, evident in the straightness of the shape's edges as the frequency increases. The maximum values for the angle and angular velocity, q and $\dot{q}$, increase as well, indicating larger and faster oscillations.

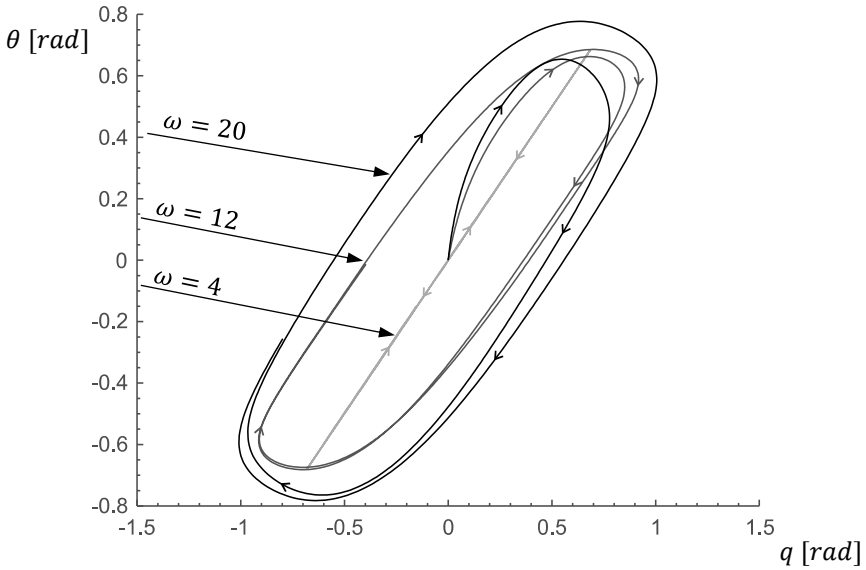

Figure 6.7 – Parametric plot of the pen's angle q and the wrist's angle θ. Three different system responses are plotted at three different input frequencies, 4, 12 and 20 rad/s. The responses were recorded over a time period of $4\pi/\omega$ of the input frequency.

In Figure 6.7, the phases are visible on the shape of the plot as well. The twisting phase is present along the co-vertices of the oval shape, while the rolling phase is present on the vertices of the oval. The magnitude of the oscillation is very noticeable in the shape of this plot. At a frequency of 4 rad/s, the oval shape has not yet formed and is rather linear, depicting a trajectory of the pen that follows the wrist's, without much room for the rolling phase, where the oscillation of the pen in relation to the fingers would take place. As the frequency increases to 12 rad/s, the shape opens up into the oval shape mentioned, with the opening illustrating the presence of the rolling phase. It grows even larger when at the frequency of 20 rad/s, validating the information gathered in Figure 6.5, where an increase in frequency lead to the increase of the oscillations, up to a threshold. The cyclicity of the system was also validated in Figure 6.7, at each of the stable frequencies.

6.4 Cyclical behavior analysis: high frequency

At higher frequencies of 46 to 58 rad/s, the response of the system evolves so as to decrease the magnitude of oscillation, $q - \theta$, as had been observed in Figure 6.5. On a parametric plot of the pen's angle and angular velocity, Figure 6.8, the system's responses are still distinguishable from each other and the inverse of Figure 6.6 can be observed, where the higher the input frequency is, the lesser the impact on q and $\dot{q}$.

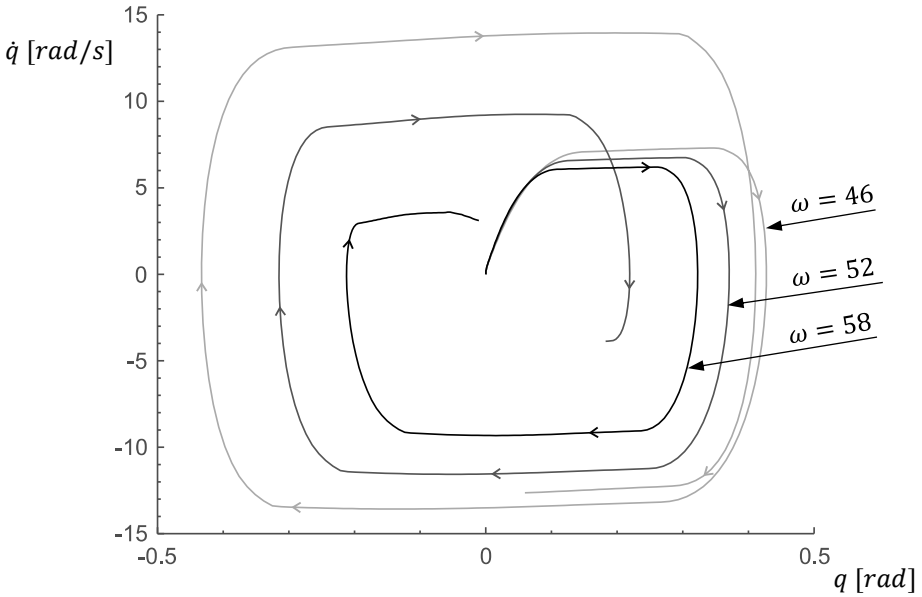

Figure 6.8 – Parametric plot of the pen's angle q and the pen's angular velocity $\dot{q}$. Three different system responses are plotted at three different input frequencies, 46, 52 and 58 rad/s. The responses were recorded over a time period of $4\pi/\omega$ of the input frequency.

It is also noticeable that, although the same period of two cycles of the input reference frequency was recorded, the pen only went through one cycle of rotation, indicating that the system is running at a frequency higher than the pen's dynamics allow and suggesting the presence of period doubling [25, 26], a phenomenon where a new periodic trajectory emerges from the already existing periodic trajectory. Investigating this phenomenon further, at the input frequency of 58 rad/s, the relevant parametric plot can be seen next, in Figure 6.9.

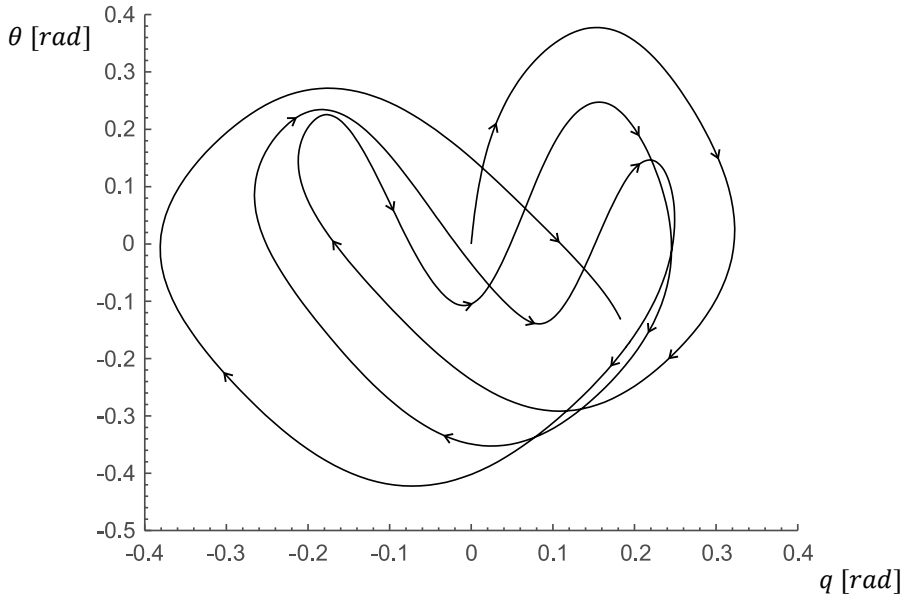

Figure 6.9 – Parametric plot of the pen's angle q and the wrist's angle θ, at the frequency of 58 rad/s. The response was recorded over a time period of $12\pi/\omega$ (6 cycles) of the input frequency.

In Figure 6.9, period doubling is clearly present, evident in the v-shave created in the plot. This shape takes form because the pen's dynamics do not allow it to oscillate at the frequency at hand. The presence of a large magnitude of oscillation is also verified, as per the "openness" of the shape in the plot, meaning that the rolling phase is very prevalent. There is little to no evidence of both angles moving in synchrony, indicating that the twisting phase is very short lived. The pen's angle does stay within bounds though, and the plot is cyclical, proving the system is stable for the frequency at hand. All in all, at high frequencies, the pen is limited to the rolling phase while being juggled between the fingers at a frequency too high for its resonant frequency.

6.5 Robustness to input amplitude and pen offset

To try the system for its robustness, its response to different amplitudes of the reference signal was recorded and plotted in the graph below, at the frequency of 19 rad/s.

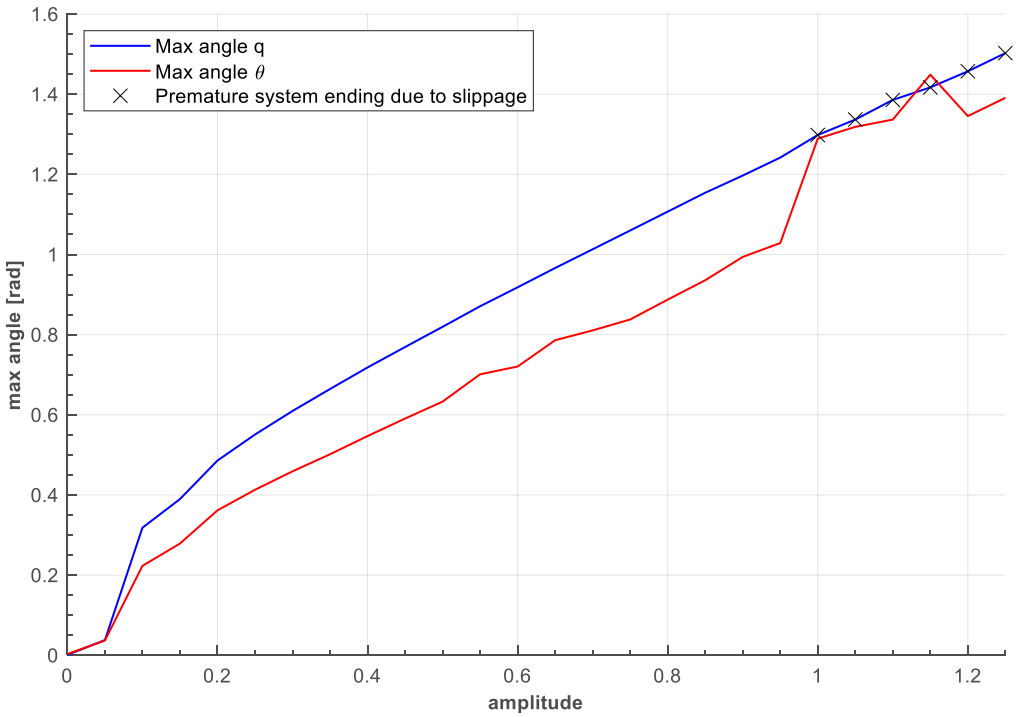

Figure 6.10 – System's response to a reference input on the pen's angle of a sine wave of amplitude A, ranging from 0 to 1.25, and frequency of $\omega = 19\,rad/s$, simulated for 5 seconds. The pen's absolute value of maximum angle, q_{max}, is drawn, in blue, while the wrist's absolute value of its maximum angle, θ_{max}, is drawn in red. Black crosses are also illustrated, representing frequencies at which the system ended prematurely due to the pen slipping off the fingertips' grasp.

In Figure 6.10 it is seen that the input amplitude has a linear relationship with both the max angle of the pen, q_{max}, and the max angle of the wrist θ_{max}. The system is stable for ranges for a range of amplitudes of 0 up to 1 and is able to produce a resonant response from the system throughout almost all this range, with an exception for amplitudes of less than 0.1, as seen by the difference of q_{max} and θ_{max}. At an amplitude of 1, the system becomes unstable and does not fully grasp the pen during the

duration of the simulation. These findings indicate that the system is very robust in terms of the reference signal's amplitude.

To further test the limits of the system, an offset was introduced in the pen's position, such that its initial starting position in the simulation was offset by some value. Thus, when grasping, the fingertips would not make contact with the vertical axis of the pen's center of mass. This would result in some extra grasping force being required to keep the pen from escaping the fingertips, given the rotating trajectory of the pen. Below is a plot of the system's response to different offset values for the initial position of the pen, with a reference signal at the frequency of 19 rad/s and an amplitude of 0.7.

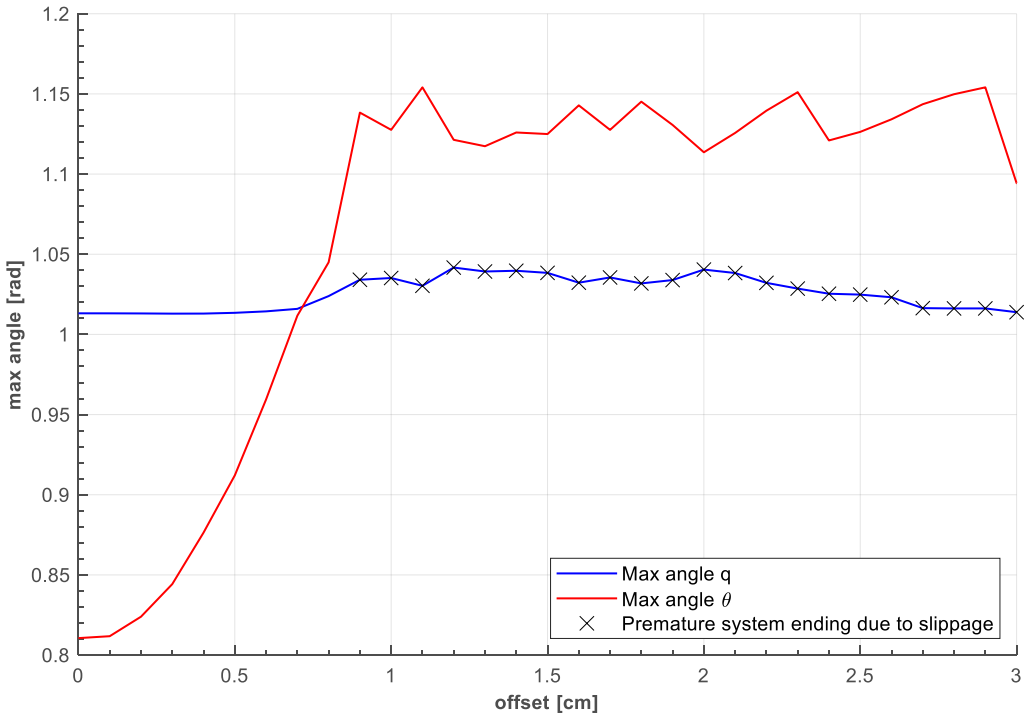

Figure 6.11 - System's response to an offset being introduced in the initial position of the pen, simulated for 5 seconds. The reference input on the pen's angle is a sine wave of amplitude $A = 0.7$ and a frequency of $\omega = 19\ rad/s$. The pen's absolute value of maximum angle, q_{max}, is drawn, in blue, while the wrist's absolute value of its maximum angle, θ_{max}, is drawn in red. Black crosses are also illustrated, representing frequencies at which the system ended prematurely due to the pen slipping off the fingertips' grasp.

From Figure 6.11 it is evident that by introducing an offset to the pen's initial position and thus altering the position of grasp on the pen, the system's response if affected. In fact, the system's magnitude of oscillation, $q_{max} - \theta_{max}$, worsens dramatically with only a few millimeters of offset on the pen's position. Although the system manages to be stable for the first few values of offset, at around 0.9 centimeters of offset (around 15% of the possible offset, half the length of the pen), the system becomes unstable and loses grasp on the pen.

Although the system manages to remain stable for some of the pen's positional offset, its response worsens considerably with it and as such, the system can then be said to be somewhat robust regarding the pen's initial position, or the position of grasp on the pen regarding its center of mass.

7 Conclusions

7.1 Achievements

This document goes into detail about how the act of grasping is sensed by the bio-mechanisms of human biology and how a robotic hand can be controlled to perform a task in which an object, a pen, is grasped and handled to perform a wiggling motion in between the fingertips.

Through sections 2 and 3 the model of the robotic hand was discussed, following strict contact models, where a novel adaptation of the existing frictional model referenced [17] was introduced. The model is bio-inspired and, as a result, follows bio-restrictions alike their flesh counterparts, except for the neurological delay on the perception and action, left for future work. These limit the access to the system's states, limiting the possibilities for the control action developed thereafter.

In sections 4 and 5, a solution for the aforementioned task was proposed. It consisted of the detection of the pen's position based on the forces felt on the fingertips followed by the controller. The controller consisted of a position controller for the position of the fingers, an impedance controller for the grasping of the pen and an impedance controller for the manipulation of the pen. The pen's position was very well predicted for low frequencies, while at higher frequencies some discrepancies do exist. However, such discrepancies did not cause the system to become unstable when operating near its resonant frequency. The impedance control proved to be smooth, and the resulting forces and torque produced were in line with the system's characteristics. Given their well-functioning, these were considered successful.

The controller was given a reference signal to follow of a sine wave with a given amplitude and frequency. It proved quite effective at using the guidance of the reference to oscillate the pen, managing to maintain stability while operating at the resonant frequency of the system, of about 19 rad/s. It also proved robust regarding the amplitude of the signal and somewhat robust when faced with an offset on the pen's initial position.

The system's response was analyzed regarding the frequency of the reference input signal as well. For low values of frequency, no oscillations occur, up to a certain threshold of around 5 rad/s. At frequencies above that, oscillations start to appear in the system. As the frequency of the system gets closer to the resonant frequency, of around 19 rad/s, the oscillations start to get larger. At around 25 rad/s the system becomes unstable (the pen escapes the fingertips' grasp) and the oscillations decrease with the increase in frequency. Then at 45 rad/s, around double the resonant frequency, the system regains its stability, and the phenomenon of period doubling can be observed.

7.2 Future work

As for the future work this essay enables, one of the main aspects is the addition of inbound and outbound delays to the system model, as discussed in section 3.3, to better simulate a true bio-inspired mechanism. This implementation is expected to be complex, as a delay of over 100 milliseconds should be enough to cause the pen to slip the fingertips' grasp.

Furthermore, this model hopes to inspire the study of various forms of dexterous movement involving the handling of objects with a non-restrictive grasp and clever use of the fingers to perform complex movements with said objects.

Appendix A

Table 5 - First twenty terms for the recursion in (2.21), as found in [14].

N	A_n	B_n
0	0	1
1	-3	2
2	3	2
3	-27	20
4	6	5
5	-759	700
6	351	350
7	-6639	7000
8	1599	1750
9	-192537	215600
10	190221	215600
11	-10993971	12512500
12	308346453	350350000
13	-6203405379	7007000000
14	894162999	1001000000
15	-41382469053	45815000000
16	136200425703	148898750000
17	-113114950247136633	121989767900000000
18	114732379536286977	121989767900000000
19	-29101190167836903	30497441975000000
20	4724140398296547	4879590716000000
⋮	⋮	⋮

References

[1] R. W. Shumaker, K. R. Walkup and B. B. Beck, Animal tool behavior: the use and manufacture of tools by animals, JHU Press, 2011.

[2] J. L. Bradshaw, "Animal asymmetry and human heredity: Dextrality, tool use and language in evolution–10 years after Walker (1980)," *British Journal of Psychology,* pp. 39-59, 1991.

[3] S. R. James, "Hominid use of fire in the Lower and Middle Pleistocene: A review of the evidence [and comments and replies]," *Current Anthropology,* pp. 1-26, 1989.

[4] K. S. Brown, "Fire as an Engineering Tool of Early Modern Humans," *Science,* pp. 859-862, 2009.

[5] T. Matsuzawa, "Primate foundations of human intelligence: a view of tool use in nonhuman primates and fossil hominids.," *Primate origins of human cognition and behavior,* pp. 3-25, 2008.

[6] R. A. Foley and R. Lewin, Principles of human evolution, John Wiley & Sons, 2013.

[7] S. KADOWAKI, "Issues of chronological and geographical distributions of Middle and Upper Palaeolithic cultural variability in the Levant and implications for the learning behavior of Neanderthals and Homo sapiens.," *Dynamics of Learning in Neanderthals and Modern Humans Volume 1,* pp. 59-91, 2013.

[8] S. Pruitt, "6 Major Breakthroughs in Hunter-Gatherer Tools," 5 August 2019. [Online]. Available: https://www.history.com/news/hunter-gatherer-tools-breakthroughs.

[9] S. A. A. Moosavian and E. Papadopoulos, "Multiple Impedance Control for Object Manipulation," *Proceedings. 1998 IEEE/RSJ International Conference on Intelligent Robots and Systems. Innovations in Theory, Practice and Applications (Cat. No. 98CH36190),* pp. 461-466, October 1998.

[10] M. Li, H. Yin, K. Tahara and A. Billard, "Learning Object-level Impedance Control for Robust Grasping and Dexterous Manipulation," *2014 IEEE International Conference on Robotics and Automation,* pp. 6784-6791, May 2014.

[11] D. J. Balkcom and M. T. Mason, "Robotic origami folding," *The International Journal of Robotics Research,* pp. 613-627, 2008.

[12] N. Uchiyama, S. Sano and K. Ryuman, "Control of a robotic manipulator for catching a falling raw egg to achieve human-robot soft physical interaction.," *2012 IEEE RO-MAN: The 21st IEEE International Symposium on Robot and Human Interactive Communication.,* pp. 777-784, 2012.

[13] J. Müller, U. Frese and T. Röfer, "Grab a mug-object detection and grasp motion planning with the Nao robot.," *2012 12th IEEE-RAS International Conference on Humanoid Robots (Humanoids 2012).,* pp. 349-356, 2012.

[14] A. S. Carvalho and J. M. Martins, "Exact restitution and generalizations for the Hunt-Crossley contact model," *Mechanism and Machine Theory,* 17 March 2019.

[15] E. Pennestrì, V. Rossi and P. Salvini, "Review and comparison of dry friction force models," *Nonlinear dynamics,* pp. 1785-1801, 21 July 2015.

[16] C. Metaldesigner and 375Designs, "grabcad," [Online]. Available: https://d2t1xqejof9utc.cloudfront.net/cads/files/b0f6e22642f96e5490f641c044c3b88d/original.zip. [Accessed 13 March 2021].

[17] H. Geyer and H. Herr, "A Muscle-Reflex Model That Encodes Principles of Legged Mechanics Produces Human Walking Dynamics and Muscle Activities," *IEEE Transactions on neural systems and rehabilitation engineering,* pp. 263-273, June 2010.

[18] M. Zhang and A. F. T. Mak, "Prosthetics and Orthotics International," *In vivo friction properties of human skin,* 1999.

[19] S. Derler, R. Huber, H. P. Feuz and M. Hadad, "Influence of surface microstructure on the sliding friction of plantar skin against hard substrates.," *Wear,* pp. 1281-1288, 2009.

[20] E. R. Kandel, J. H. Schwartz, T. M. Jessell, S. A. Siegelbaum and A. J. Hudspeth, Principles of Neural Science, New York: McGraw-hill, 2000.

[21] E. R. Baldwin, P. M. Klakowicz and D. F. Collins, "Wide-pulse-width, high-frequency neuromuscular stimulation: implications for functional electrical stimulation.," *Journal of Applied Physiology,* pp. 228-240, 2006.

[22] C. Donnely, "Modulation of torque evoked by wide-pulse, high-frequency neuromuscular electrical stimulation and the potential implications for rehabilitation and training," *Scientific Reports,* pp. 1-13, 2021.

[23] K. Ogata, Modern control engineering, 2010.

[24] S. A. Campbell, "Limit cycles, tori, and complex dynamics in a second-order differential equation with delayed negative feedback.," *Journal of Dynamics and Differential Equations,* pp. 213-236, 1995.

[25] C. Tresset, P. Coullet and E. de Faria, "Period doubling," *Scholarpedia,* p. 3958, 2014.

[26] D. W. Jordan and P. Smith, Nonlinear ordinary differential equations: an introduction to dynamical systems., USA: Oxford University Press, 1999.